

**Assessing the impacts of climate change on hydrological processes  
in the upper Genale River basin, Ethiopia**

Author

Shigute, Mehari, Alamirew, Tena, Abebe, Adane, Ndehedehe, Christopher E, Kassahun, Habtamu Tilahun

Published

2024

Journal Title

Environmental Earth Sciences

Version

Accepted Manuscript (AM)

DOI

[10.1007/s12665-024-11586-2](https://doi.org/10.1007/s12665-024-11586-2)

Rights statement

This work is covered by copyright. You must assume that re-use is limited to personal use and that permission from the copyright owner must be obtained for all other uses. If the document is available under a specified licence, refer to the licence for details of permitted re-use. If you believe that this work infringes copyright please make a copyright takedown request using the form at <https://www.griffith.edu.au/copyright-matters>.

Downloaded from

<https://hdl.handle.net/10072/430829>

Griffith Research Online

<https://research-repository.griffith.edu.au>

1 **Assessing the Impacts of Climate Change on Hydrological Processes in the Upper Genale**  
2 **River Basin, Ethiopia**

3 Mehari Shigute<sup>a,b</sup>, Tena Alamirew<sup>a,c</sup>, Adane Abebe<sup>d</sup>, Christopher E. Ndehedehe<sup>e,f</sup>, Habtamu  
4 Tilahun Kassahun<sup>e</sup>

5 <sup>a</sup> *Ethiopian Institute of Water Resources (EIWR), Addis Ababa University, P. O. Box 150461, Addis Ababa, Ethiopia.*

6 <sup>b</sup> *Natural Resource Management, Dilla University, P. O. Box 419, Dilla, Ethiopia*

7 <sup>c</sup> *Water and Land Resource Center (WLRC), Addis Ababa University, P. O. Box 3880, Addis Ababa, Ethiopia*

8 <sup>d</sup> *Arba Minch Water Technology Institute: Arba Minch University, P. O. Box 21, Arba Minch, Ethiopia*

9 <sup>e</sup> *Australian Rivers Institute, Griffith University, Nathan, QLD 4111, Australia*

10 <sup>f</sup> *Griffith School of Environment & Science, Griffith University, Nathan, QLD 4111, Australia*

11

12 **Abstract**

13 The aim of this research is to assess the impact of future climate change on hydrological parameters (e.g., precipitation,  
14 temperature, etc.) in Ethiopia's upper Genale River basin. Future climate scenarios for the 2021–2050 and 2051–2080  
15 periods were developed from four different GCM–RCM combinations of CORDEX-Africa projections using the  
16 Representative Concentration Pathways (RCP 4.5 and RCP 8.5). These climate models were bias corrected and used  
17 as input to the Soil and Water Assessment Tool (SWAT) model. During the 2030s (2021–2050) and 2060s (2051–  
18 2080), under the two RCPs, the projected precipitation in the annual and seasonal periods tends to decrease while  
19 temperatures increase. The simulated result revealed a significant change in hydrological components (e.g., During  
20 the 2060s), under the RCP4.5 scenario, CNRM-CM5 climate model runoff, ground water flow, and total water yield  
21 increased by 24.47%, 27.98%, and 28.56%, respectively. On the contrary, during the 2060s under the MIROC5 climate  
22 model, runoff, ground water flow, and total water yield reduced by 20.84%, 34.34%, and 25.8%, respectively. The  
23 annual hydrological components of the study area under MPI-ESM-LR, EC-EARTH, and MIROC5 showed a decrease  
24 in total water yield, surface runoff, ground waterflow, and lateral flow. However, due to a rise in temperature,  
25 evapotranspiration showed an increase up to 8.1% under all climate models (MPI-ESM-LR, EC-EARTH, CNRM-  
26 CM5, and MIROC5). The reduction in rainfall, which coincides with rising temperatures, is expected to reduce annual  
27 water yield, surface runoff, ground waterflow, and lateral flow by up to 39.8%, 39%, 50%, and 40.1%, respectively,  
28 across MPI-ESM-LR, EC-EARTH, and MIROC5 scenarios for the entire study basin in future projections. Our study  
29 helps to give a better insight into understanding climate change in watershed and can benefit the planning of water  
30 resources by strengthening adaptation strategies against the impacts of future climate change.

31 **Keywords:** Upper Genale River basin, Climate change, Regional climate models, Hydrological processes, SWAT  
32 model.

33

34 **\*Corresponding author at:** Dilla University, Natural Resource Management, Dilla, Ethiopia  
35 E-mail address: meharishigute@gmail.com (Mehari Shigute).

36

37

38

39 **1.Introduction**

40 Emissions of greenhouse gases (GHGs) into the atmosphere have increased since the pre-industrial  
41 era, primarily due to the expansion of intensive agriculture, industrialization, the utilization of  
42 fossil fuels, and urbanization (Hussain et al., 2018; IPCC., 2014; Shrestha, 2014). Changes in GHG  
43 concentrations in the atmosphere primarily tend to raise the temperature (Syukuro, 2019). The  
44 change in climate has caused the mean temperature to rise across the globe. Since the 1900s, it has  
45 risen by about 0.8°C, and by the end of the 21st century, it is expected to rise by 1.4–2.0°C (IPCC,  
46 2013). A warmer climate accelerates and changes the hydrological cycle, causing long term  
47 changes in evapotranspiration, rainfall, and runoff volume and timing, and resulting in negative  
48 impacts on natural water resources in a catchment (Dariane & Pouryafar, 2021; Ketema &  
49 Dwarakish, 2021).

50 Climate change has also had an effect on natural and human systems all over the world (IPCC.,  
51 2014). The extent of the adverse impacts, however, varies substantially across continents,  
52 countries, and socioeconomic strata, due to the adverse direct impacts on national GDP growth,  
53 food security, and low adaptive and high exposure capacity to climate change. The impacts are far  
54 more severe for African countries in general, and Ethiopia in particular (Asfaw et al., 2018; Bewket  
55 et al., 2015; Dosio et al., 2022; EPCC, 2015; Girvetz et al., 2019; IPCC., 2014; Serdeczny et al.,  
56 2017).

57 Climate change has negatively affected Africa in several ways (Godfrey & Tunhuma, 2020;  
58 Welborn, 2018). This includes increased frequency and severity of natural disasters, decreased  
59 rainfall amount and distribution, and exacerbated existing water stress. All of these have  
60 significant impact on the functional operation of existing water resource development projects,  
61 ecological systems, and agricultural development (Chaemiso et al., 2016; Emiru et al., 2022).  
62 Moreover, frequent occurrences of hydrological extremes and high rainfall variability, along with  
63 rapidly growing populations and alarmingly increasing food and water demands, have an effect on  
64 the health and livelihoods of Africans (Dibaba et al., 2019).

65 Throughout the world numerous studies on the impact of climate change on hydrological responses  
66 have been undertaken (Awotwi et al., 2021; Bekele et al., 2019; Bekele et al., 2021; Birkinshaw et  
67 al., 2017; Eisner et al., 2017; Galata et al., 2021; Lotfirad et al., 2021; Mengistu et al., 2020;  
68 Näschen et al., 2019; Takele et al., 2022; Tessema et al., 2021; Worku et al., 2021; Worqlul et al.,

69 2018; Zhang et al., 2018). Many of these studies found that climate change influenced and will  
70 continue to negatively affect the hydrologic characteristics of a catchment. For instance, Näschen  
71 et al. (2019) analyzed the impacts of climate change on water resources in Tanzania's Kilombero  
72 Catchment. They reported that the mean annual water yield and surface runoff increased by 61.6%  
73 and 67.8%, respectively. Studies undertaken in other regions (e.g., Yangtze basin of China), which  
74 used the Representative Concentration Pathways (RCP 8.5) scenario revealed that the annual basin  
75 discharge changes from -29.8 to +16.0% (Birkinshaw et al., 2017). Changes in the magnitude and  
76 pattern of temperature, rainfall, and climate on both local and global scales affect the rate and  
77 occurrence of hydrological characteristics in a basin (Daba & You, 2020).

78 Climate change is also having a negative effect on water resources in Ethiopia, a largely rain-fed  
79 agricultural region in Africa. The impact is primarily caused by shifting rainfall patterns, rising  
80 temperatures, and increased atmospheric water demand (Bewket, et al., 2015). Temperature rise  
81 as well as alterations in precipitation patterns are two of the most important climate change  
82 variables that have a direct impact on almost all other hydrologic processes (Daba & You, 2020;  
83 Ketema & Dwarakish, 2021; Musie et al., 2020; Tessema et al., 2021). A study by Daba and You  
84 (2020) in Ethiopia's upper Awash basin revealed that changes in temperature and rainfall under  
85 both RCP4.5 and RCP8.5 scenarios for all future periods (2020s, 2050s, and 2080s) are expected  
86 to affect surface runoff, streamflow, and total water yield within the basin. Climate change also  
87 has an impact on water resource planning and management through changes in the amount and  
88 seasonal patterns of flows in streams (Musie et al., 2020). Hence, assessing the effect of climate  
89 change on water resources at the small and large watershed scales by combining climate and  
90 hydrological models is essential for understanding climate change vulnerability and designing  
91 ecologically sound water resource management strategies.

92 Even though various studies of the impact of climate change on hydrologic analysis have recently  
93 been carried out in various parts of Ethiopia using high-resolution ensembles of regional climate  
94 predictions generated by Coordinated Regional Climate Downscaling Experiment (CORDEX)  
95 (Bekele et al., 2021; Daba & You, 2020; Eromo et al., 2016; Galata et al., 2021; Ketema &  
96 Dwarakish, 2021; Mengistu et al., 2020; Tessema et al., 2021; Worqlul et al., 2018), in depth  
97 scientific studies on the quantitative impact of climate change on water resources based on the  
98 RCP have not been conducted in the study basin. Furthermore, studying climate change impact on

99 hydrological variables, particularly total water yield, surface runoff, groundwater flow, and  
100 evapotranspiration, by using hydrological models and downscaled climatic data are crucial for arid  
101 and semi-arid regions. Water resources mainly runoff and streamflow, are extremely impacted by  
102 climate change. A minor change in climate variables can cause significant changes in hydrological  
103 components and, as a result, changes in regional water resources (Daba & You, 2020). Moreover,  
104 hydrological characteristics vary by location, and the effects of climate change on hydrology vary  
105 greatly across regions (Abeysingha et al., 2020); hence, it is vital to conduct such study in arid and  
106 semi-arid regions in order to develop and implement sustainable management of scarce water  
107 resources and appropriate climate change adaptation and mitigation strategies (Galata et al., 2021;  
108 Musie et al., 2020; Worqlul et al., 2018).

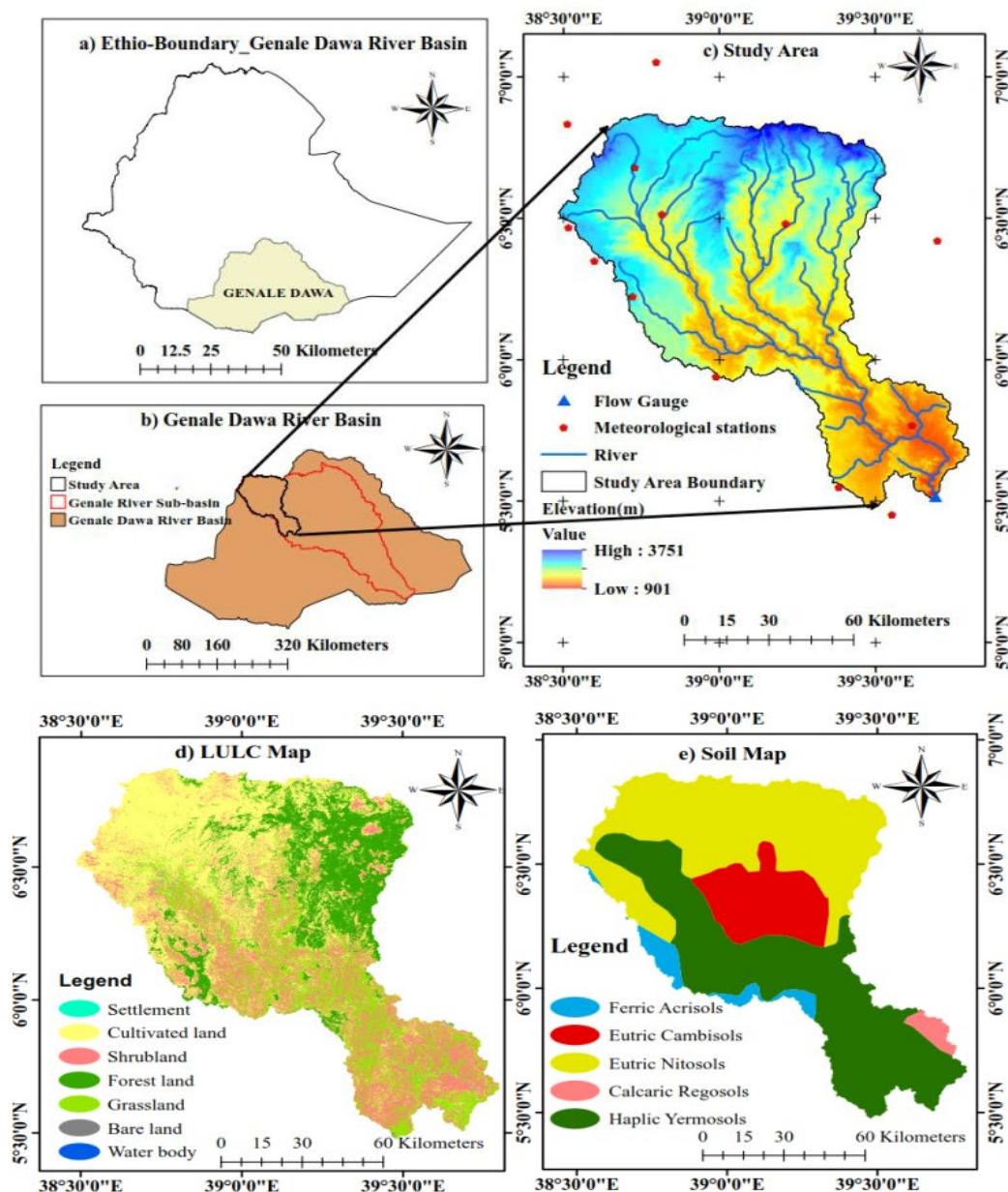
109 Therefore, this study was mainly designed to evaluate climate change impact on hydrological  
110 processes over the study area of the upper Genale River basin. The Genale River is a multi-purpose  
111 river on which different water-based projects have been implemented. The projects include many  
112 proposed and existing hydropower power plants, small- and large-scale irrigation schemes, and  
113 fish farming at the different parts of the river. The basin is characterized by a variety of topographic  
114 and climatic regimes. Knowledge of the impact of climate change on hydrological characteristics  
115 in a river basin is important for planning prospective climate change adaptation as well as  
116 mitigation actions. Additionally, the results of this research may be used to develop and execute  
117 new strategies for efficient water resource management, utilization, and development in order to  
118 prevent water scarcity in the area. Therefore, this study was undertaken with the aim of evaluating  
119 the hydrological characteristics of the upper Genale River basin under the effect of climate change  
120 using the SWAT model and the CORDEX-Africa Regional Climate Model (RCM) under RCP4.5  
121 and RCP8.5 climate scenarios.

## 122 **2.MATERIALS AND METHODS**

### 123 **2.1 Study Area Description**

124 The Genale Dawa basin is located in Ethiopia's southern region and includes parts of the regional  
125 states of Oromia, Somali, and Southern Nations, Nationalities, and Peoples' (SNNP) (Figs. 1, a–  
126 c). The basin has an approximate area of 172,713km<sup>2</sup>. Geographically, it lies North of 3°30' - 7°  
127 20' latitude and East of 37° 05' - 43° 20' longitude (Awulachew et al., 2007; MoWE, 2007a) (Fig.  
128 1 b). The upper Genale River, the study basin, is found in the upper central area of the Genale

129 Dawa River basin. It has an area of approximately 10,582.19 km<sup>2</sup> and is situated between North  
 130 of 6° 52' and 5° 28' latitude and East of 38° 30' and 39° 45' longitude (Fig. 1c).



131  
 132 Fig. 1. Study area Map (a) Ethiopia boundary (b) Genale Dawa River basin (c) Upper Genale  
 133 River basin (Study area) (d) land cover map, and (e) Soil map. Source (Shigute et al., 2022)

134 The basin has a three-season type I bimodal annual rainfall cycle in the highlands (northern parts)  
 135 and a double dry and wet season type II in the lowlands (southeastern). The three wet seasons are  
 136 known locally as belg (March, April, and May), kiremt (June-September), and meher (September,  
 137 October, and November)(MoWE, 2007a). The double wet season in the southern and southeastern

138 parts is from March to May and from September to November (Degefu et al., 2021; MoWE, 2007).  
139 The annual mean rainfall, minimum and maximum temperatures range from 1617.7mm to 591mm,  
140 6.9 to 16.2 °C, and 18.9 to 27.7°C, respectively (Shigute et al., 2023).

## 141 **2.2 Input Data**

### 142 **Input Data for SWAT Model**

143 To assess the SWAT model performance and the effect of climate change on the hydrologic  
144 characteristics of the watershed, spatial and temporal data were used.

#### 145 **2.2.1 spatial data**

146 SWAT model utilizes spatial data such as the Digital Elevation Model (DEM), Land Use Land  
147 Cover (LULC), and soil maps. The DEM, obtained from the USGS website at a resolution of 30m,  
148 was used to determine the basin boundary, sub-basins, and various characteristics (e.g., elevation,  
149 slope gradient, river network, etc), and the hydrologic response unit (Fig. 1c). The classified LULC  
150 map was obtained from Shigute et al. (2022), revealing major land categories as cultivated land  
151 (47%), shrubland (19.53%), forest land (13.53%), and grassland (18.9%) (Fig. 1 d). The soil map  
152 was acquired from the Food and Agricultural Organization (FAO). The SWAT database and the  
153 Genale Dawa River basin master plan, developed by Ethiopia's Ministry of Water Resources  
154 (MoWE, 2007b), were used to extract, verify, and compare the necessary soil physical and  
155 chemical properties. The soil types in the study area include Calcaric Regosols (1.6%), Ferric  
156 Acrisols (3.7%), Eutric Cambisols (13.1%), Eutric Nitosols (40.3%), and Haplic Yermosols  
157 (41.4%) (Fig. 1e).

158

#### 159 **2.2.2 Temporal data**

##### 160 **Climate data**

161 To run the SWAT model, daily rainfall data (1984–2016) for ten stations and minimum and  
162 maximum temperature data for five stations were obtained from the National Meteorological  
163 Agency of Ethiopia (NMA) (Table 1). Data for the Harokelo, Bidere, and Arbegona locations were  
164 extracted from the ENACTS dataset. The dataset, which has a resolution of 4 x 4 km, was  
165 constructed by combining data from satellite estimates from NASA (the US National Aeronautics  
166 and Space Administration) and EUMET-SAT (the European Organization for the Exploitation of  
167 Meteorological Satellites) with station records from nearby locations (Dinku et al., 2014, 2016).

168 The effectiveness of ENACTS has been evaluated at numerous stations across the nation, and it  
 169 has turned out to be effective (Alemayehu & Bewket, 2017; Dinku et al., 2014, 2016).

170 The Multivariate Imputation by Chained Equations (MICE) algorithm as explained in van Buuren  
 171 & Groothuis-Oudshoorn, (2011) was used to generate and fill the missing values, and then the data  
 172 was used for further analyses. To ensure the data's quality and reliability, homogeneity tests were  
 173 performed. The standard normal homogeneity test (SNHT) (Alexandersson, 1986), the Buishand  
 174 range test (Buishand, 1982), the Von Neumann ratio test (von Neumann, 1941), and the Pettitt test  
 175 (Pettitt, 1979) were the four absolute statistical homogeneity tests used. The details of the analysis  
 176 results in Shigute et al. (2023) showed that the data were homogeneous and could be used for  
 177 further analyses.

178 In addition, the ARCSWAT weather generator (WGNMarker 4) was used to generate weather  
 179 elements such as wind speed, relative humidity, and solar radiation. The model was then initialized  
 180 using weather data from 1984 to 1986. The SWAT analysis was then performed on data from 1987  
 181 to 2016.

182 Table 1: Summary of the study area meteorological stations and their geographical locations.

Name of Stations	Latitude ( N°)	Longitude ( E°)	Altitude (m)	Rainfall	Temperature
				Period	Periods
Telamokentise	6°50'1"	38°30'38"	1911	1990-2016	
Yirba Muda	6°13'17"	39°35'43"	2560	1987-2016	
Woreka	6°30'6"	39°12'45"	2450	1987-2016	
Bore	6°20'30"	38°38'29"	2712	1984-2016	
Kibre Mengist	5°53'46"	38°58'1"	1680	1984-2016	
Bidere	5°46'19"	39°36'46"	1400	1984-2016	1984-2016
Arbegona	6°40'48"	38°43'30"	2600	1984-2016	1984-2016
Harokelo	5°33'19"	39°23'17"	1600	1984-2016	1984-2016
Hager Selam	6°30'47"	38°31'18"	2809	1984-2016	1984-2016
Neghele	5°26'1"	39°35'43"	1544	1984-2016	1984-2016

183

184 **Flow data**

185 For model calibration and validation, the daily streamflow data recorded at Chenemassa gauging  
 186 station from 1984 to 2011 was collected from the Ethiopian Ministry of Water, Irrigation, and

187 Energy (MoWIE). To estimate missing values, multiple imputation was used, which is the best  
188 method for estimating missing values in flow data (Sattari et al., 2017).

### 189 **2.3 GCM-RCM and scenario selection**

190 To assess future climate change impacts on the hydrologic characteristics of the study watershed,  
191 future precipitation and temperature data from CORDEX Africa RCMs were obtained from the  
192 ESGF website (<https://esgdn1.nsc.liu.se/esgf>). For this study, three different RCMs (KNMI  
193 Regional Atmospheric Climate Model, version 22 (RAMO22 T), Rossby Center regional  
194 atmospheric model (RCA4), and Regional Climate Limited-area modeling (CCLM)) and four  
195 downscaled GCM driving models (EC-EARTH, CNRM-CM5, MIROC5, and MPI-ESM-LR) of  
196 CMIP5 (Climate Model Inter-comparison Project Phase 5) were used in combination. These  
197 resulted in four GCM-RCM combinations of CORDEX-Africa projections under two RCPs (4.5  
198 and 8.5) (Table 2), which were used for impact assessment. The details of the two RCPs scenarios  
199 are explained by the IPCC (IPCC, 2014). The choice of the GCM-RCM model was made in  
200 consideration of other studies of the effects of climate change on east Africa, particularly in various  
201 regions of the Ethiopia river basin, as well as how well the climate models represent past and  
202 present climate, their resolution, and other related factors (Adera & Alfredsen, 2020; Adugna et  
203 al., 2021; Bekele et al., 2021; Ketema & Dwarakish, 2021; Mengistu et al., 2020; Musie et al.,  
204 2020; Tessema et al., 2021; Worku et al., 2020)

205 The spatial resolution of the CORDEX-Africa domain is 0.44° by 0.44°, which is about 50 km by  
206 50 km. The data covers from the years 1951 to 2100, with a historical time frame from 1951 to  
207 2005 and a future projection from 2006 to 2100 (Musie et al., 2020). In this study, to assess the  
208 change in patterns of climate data, the baseline scenario period (1987-2016) and the future scenario  
209 period (2021-2100) were used. The future scenarios were divided into two different periods of  
210 time with 30-year intervals, such as 2021-2050 (the 2030s) and 2051-2080 (2060s).

211 Table 2. Descriptions of selected GCM - RCM climate models

GCM Name	RCM	INSTITUTION
CNRM-CM5	CCLM4-8-17-V1	Climate Limited-area Modelling Community
EC-EARTH	RACMO22T_v1	Royal Netherlands Meteorological Institute
MIROC5	SMHI-RCA4_V1	Swedish Meteorological and Hydrological Institute
MPI-ESM-LP	CCLM4-8-17-V1	Climate Limited-area Modelling Community

212

### 213 **Bias correction**

214 To assess the likely effect of climate change on the watershed's hydrological aspects using the  
215 SWAT model, bias-corrected RCM data under RCP4.5 and RCP8.5 scenarios were used. The  
216 process of bias correction involves adjusting the raw output of a climate model using a  
217 transformation algorithm, under the presumption that the algorithm used to parametrize and correct  
218 the current climate will also be applicable to future scenarios (Yeboah et al., 2022).

219 For this study, to bias-correct and extract data from the RCM model, CMhyd tool was used  
220 (Rathjens et al., 2016). To correct the maximum and minimum temperature and precipitation data,  
221 the linear scaling method was selected from the available bias correction techniques in the CMhyd  
222 software. Because of its simplicity, accuracy, and ease of application, this method has been widely  
223 used to correct GCM-RCMs in various parts of the world (Abera & Gebeyehu, 2023; Azman et  
224 al., 2022; Galata et al., 2021; Mahmood et al., 2018; Mahmood & Babel, 2013; Mahmood & Jia,  
225 2017; Shrestha et al., 2017; Takele et al., 2022). Furthermore, the method works well for climate  
226 change-related water resource research (Takele et al., 2022).

227 To adjust the RCM simulation of temperature and rainfall, the linear scaling method employs  
228 additive and multiplicative factors, respectively. The factors are produced by comparing the  
229 measured data to the corresponding historical RCM simulations (Worku et al., 2020). The detailed  
230 description of the method is available on the previous work of Luo et al. (2018) and Teutschbein  
231 & Seibert (2012).

### 232 **2.4 SWAT model description and set up**

233 The SWAT is a semi-distributed, physically based hydrologic model that operates on a continuous  
234 time-step (Arnold et al., 2012). The model is developed to simulate the climate change effects on  
235 hydrology, land management, and movement of agricultural chemicals and sediment of a wide and  
236 complex basin (Arnold et al., 1998; Taylor et al., 2016). The hydrology is simulated in two major  
237 ways: The Land Phase, which controls the nutrient, pesticide, sediment loaded, and water transport  
238 to each channel from sub-watersheds, and the Water or Routing Phase that controls the movement  
239 of flow up to the basin outlet. The SWAT model simulates the hydrologic phenomena of the land

240 phase using the water balance equation shown as follows (Narsimlu et al., 2015; Neitsch et al.,  
241 2011):

$$242 \quad SW_t = SW_o + \sum_{i=1}^t (P_{day} - Q_{surf} - E_a - Q_{gw} - W_{seep}) \quad (1)$$

243 where  $SW_t$  and  $SW_o$  represent the final and initial soil water content on day  $i$  (mm),  $W_{seep}$ ,  $Q_{gw}$ ,  
244  $E_a$ ,  $Q_{surf}$ , and  $P_{day}$  represent the amount of water entering the vadose zone from the soil profile,  
245 return flow, evapotranspiration, surface runoff, and precipitation, respectively on day  $i$ (mm), and  
246  $t$  is time (days).

247 The SWAT model uses either the USDA Conservation Service Curve Number (SCN-CN) or the  
248 Green and Amp method for calculating surface runoff produced in the watershed (Neitsch et al.,  
249 2011). For this study, the SCN-CN technique (Equation 2) was applied to estimate runoff for  
250 each HRU (Arnold & Fohrer, 2005).

$$Q_{surf} = \frac{(P_{day} - 0.2S)^2}{(P_{day} + 0.8S)} \quad (2)$$

251 Where,  $Q_{surf}$ ,  $P_{day}$ , and  $S$  represent, daily depth of accumulated surface runoff (mm), the daily  
252 rainfall (mm), and retention parameter, respectively. Based on equation 2, runoff happens in a  
253 watershed when  $P_{day} > 0.2S$ .

254 In relation to the CN, the parameter  $S$  is calculated using Equation 3. The retention parameter,  $S$ ,  
255 is affected by slope, soil type, and land management practices.

$$256 \quad S = \frac{254(100 - CN)}{CN} \quad (3)$$

257 Where,  $CN$  is the curve number for the day. During model calibration process,  $CN$  is the main  
258 parameter that determine the catchment runoff (Arnold et al., 2012).

259 The SWAT model has three different approaches for calculating evaporation: the Hargreaves,  
260 Priestly-Taylor, or Penman-Monteith methods (Neitsch et al., 2011). For this study, because of the  
261 limited availability of data and the simplicity of the method, the Hargreaves method was applied  
262 (Hargreaves & Samani, 1985).

263  $ET_o = 0.0023 * Ra * (T_{max} - T_{min})^{0.5} * (T_{avg} + 17.8)$  (4)

264 Where,  $ET_o$ ,  $Ra$ ,  $T_{max}$ ,  $T_{min}$ , and  $T_{avg}$  represent, reference evapotranspiration, extraterrestrial  
265 radiation [mm/day], maximum, minimum, and average temperature [°C].

## 266 **2.5 Sensitivity analysis**

267 Hydro-climatic parameters from 1984 to 2016 were used to simulate the hydrological  
268 characteristics of the study watershed. The first three years of data (1984-1986) were used to  
269 initialize the SWAT model, while data from 1987-2016 were employed for sensitivity and  
270 calibration analysis.

271 Identifying the most sensitive parameters in The SWAT model is critical for calibration and  
272 validation streamflow (Abbaspour et al., 2018; Chimdessa et al., 2019). For this study, to  
273 differentiate the most sensitive ones, twenty-one flow parameters were meticulously chosen from  
274 the literature and the SWAT-CUP. Then, by using the objective function,  $P$ -values and  $t$ -stat,  
275 multiple regression methods with Latin hypercube method, sensitivities of parameters were  
276 determined. The  $p$ -values and  $t$ -stat show the level and degree of sensitivity to flow parameters,  
277 respectively. The larger  $p$ -values indicating less sensitivity and smaller values indicating greater  
278 sensitivity. Small absolute  $t$ -stat values imply lower sensitivity, while large values reveal higher  
279 sensitivity (Abbaspour, 2015; Narsimlu et al., 2015).

## 280 **Calibration and Validation of SWAT Model**

281 Streamflow data from the Chenemasa gauging station was used to calibrate and validate the SWAT  
282 model. Calibration and validation were performed using streamflow data from 1987 to 2002 and  
283 2003 to 2011, respectively. To calibrate and validate the model, the SWAT-CUP2012 software's  
284 sequential uncertainty fitting (SUFI-2) algorithm was used (Abbaspour, 2015). SUFI-2, is the most  
285 widely applied program in Ethiopia for model calibration, validation, and sensitivity analysis  
286 (Abraham & Nadew, 2018; Bekele et al., 2021; Belihu et al., 2020; Bizuneh et al., 2021; Bogale,  
287 2021; Mengistu et al., 2020; Takele et al., 2022; Teklay et al., 2020; Tessema et al., 2021).

## 288 **Evaluation of SWAT model performance**

289 The statistical parameter values of Nash-Sutcliffe efficiency (NSE), coefficients of determination  
290 ( $R^2$ ), and percent bias (PBIAS) were used to assess the performance of the SWAT model. These

291 statistical units are the most commonly used parameters to assess the performance of models  
 292 (Akoko et al., 2021; Shukla & Gedam, 2018). Statistical indices of *PBIAS*,  $R^2$ , and *NSE* were  
 293 calculated using Equations 5, 6, and 7 respectively

294 The amount of the total variance in the observed data that the model can explain is indicated by  
 295 the regression coefficient ( $R^2$ ). The greater the agreement between the observed and the simulated  
 296 flow, the closer the value of  $R^2$  is to 1. Equation 4 is used to calculate  $R^2$  as shown below:

$$297 \quad R^2 = \left\{ \frac{\sum_{i=1}^N (O_i - \bar{O})(P_i - \bar{P})}{\left[ \sum_{i=1}^N (O_i - \bar{O})^2 \right]^{0.5} \left[ \sum_{i=1}^N (P_i - \bar{P})^2 \right]^{0.5}} \right\}^2 \quad (5)$$

298 Nash-Sutcliffe coefficient (Nash & Sutcliffe, 1970) described in Equation 5 was used to determine  
 299 how the observed data and simulated output closely fit in 1:1 line.

$$300 \quad NSE = 1 - \frac{\sum_{i=1}^N (O_i - P_i)^2}{\sum_{i=1}^N (O_i - \bar{O})^2} \quad (6)$$

301 According to Moriasi et al. (2007), the percent of bias (*PBIAS*) was used to estimate how much  
 302 the measured values would differ from the values of the simulated output of counterparts. To  
 303 calculate *PBIAS* equation 7 was used.

$$304 \quad PBIAS = \frac{\sum_{i=1}^N (O_i - P_i)}{\sum_{i=1}^N (O_i)} * 100 \quad (7)$$

305 Where  $\bar{P}$  and  $\bar{O}$  represent mean simulated and measured data;  $P_i$  and  $O_i$  represent simulated and  
 306 measured data; and  $N$  represents the number of compared values.

307 According to Moriasi et al. (2007), the performance of the model is acceptable when the  $R^2$  value  
 308 exceeds 0.6, *NSE* greater than 0.5, and *PBIAS* falls within a range of  $\pm 25\%$ . The value of the *NSE*  
 309 varies from  $-\infty$  to 1, and where the *NSE* is close to 1, the model performs best. The value of  $R^2$   
 310 ranges between 0 to 1, where  $R^2$  close to 1 specifies less error. On the other hand, the model  
 311 simulation works best when *PBIAS* is close to 0. The model under- and overestimates the  
 312 simulation, respectively, as indicated by the positive and negative *PBIAS* values (Nasiri et al.,  
 313 2020).

## 314 2.5 Analysis of future climate characteristics

315 To analyze the RCM simulations of climate characteristics, seasonal and annual future temperature  
 316 and precipitation time series data from the selected GSM were used. A few techniques have been  
 317 developed to analyse climate characteristics. For this study, trend analysis using MK test and Sen's  
 318 slope estimator were used.

### 319 **2.5.1 Trends**

320  
 321 For this study, prior to Mann-Kendall trend analysis, temperature and precipitation time series  
 322 were tested for autocorrelation at a 5% significance level, which is critical for accurate trend  
 323 analysis. To handle serial correlation, we used a well-known method, specifically the Bias-  
 324 corrected prewhitening (BCPW) technique proposed by Hamed (2009), which is well-known for  
 325 its effectiveness in hydrologic data trend analysis.

326  
 327 Sen's slope estimator and the Mann-Kendall (MK) test were used to identify and measure potential  
 328 trends in seasonal and annual temperature and precipitation time series data. In the MK test, the  
 329 test statistic,  $S$ , being positive or negative signifies an increasing or decreasing trend, and it is  
 330 computed as outlined by Kendall (1975) and Mann (1945)

$$331 \quad 332 \quad S = \sum_{i=1}^{n-1} \sum_{j=i+1}^n \text{sgn}(x_j - x_i) \quad (8)$$

333  
 334 Where,  $x_i$  and  $x_j$  represent the time series data in the years  $i$  and  $j$  ( $j > i$ ), respectively;  $N$  is the length  
 335 of the time series, and  $S$  is the Mann-Kendal's test statistics. The sign function is computed by  
 336 Equation 9.

$$337 \quad 338 \quad \text{sgn} = (X_j - X_i) = \begin{cases} +1 & \text{if } (X_j - X_i) > 0 \\ 0 & \text{if } (X_j - X_i) = 0 \\ -1 & \text{if } (X_j - X_i) < 0 \end{cases} \quad (9)$$

339 According to Kendall (1975) and Mann (1945), the 'S' statistic is approximately normally  
 340 distributed with the mean, and  $E(S)$  becomes 0 when the number of observations exceeds 10. In  
 341 this case, Equation 10 computes the  $Var(S)$  (variance statistic) as:

$$342 \quad Var(S) = \frac{1}{18} [N(N-1)(2N+5) - \sum_{p=1}^q tp(tp-1)(2tp+5)] \quad (10)$$

343 Where,  $N$  represents the number of data points and  $tp$  and  $q$  represent the number of data points in  
 344 the  $i^{\text{th}}$  tied group and the number of tied groups in the data set, respectively.

345  
346  
347  
348

When the sample size is greater than ten, Equation 11 is used to compute the MK standardized test statistic, ZMK (Kendall, 1975; Mann, 1945).

$$Z_{MK} = \begin{cases} \frac{S-1}{\sqrt{\text{Var}(S)}} & \text{if } S > 0 \\ 0 & \text{if } S = 0 \\ \frac{S+1}{\sqrt{\text{Var}(S)}} & \text{if } S < 0 \end{cases} \quad (11)$$

349  
350 The standardized test statistic, ZMK, was applied to assess whether or not there was a statistically  
351 significant trend. The alternate hypothesis ( $H_a \neq \mu$ ) and the null hypothesis ( $H_o = \mu = \mu_o$ ) in this  
352 trend test state that there is a monotonic (upward or downward) trend or no monotonic trend  
353 observed in the dataset over time, respectively.

#### 354 **Estimating the Magnitude of the Trend**

355 Sen's slope estimator was used to compute the slope of seasonal and annual rainfall and  
356 temperature changes. Theil (1950) and Sen (1968) developed Sen's slope method to estimate the  
357 magnitude of a linear trend in a time series. As a result, the linear model,  $f(t)$ , can be expressed as  
358 Equation 12:

$$359 \quad f(t) = Qt + \beta \quad (12)$$

360 Where  $Q$  and  $\beta$  indicate the slope and the intercept of the trend line.

361 To determine the slope estimate,  $Q$ , the slopes of all data value pairs are calculated as follows:

$$362 \quad Q_i = \frac{Y_j - Y_i}{X_j - X_i} \quad i = 1, 2, \dots, N, j > i. \quad (13)$$

363 where,  $X_i$  and  $Y_i$  represent the  $i^{th}$  observation's time and its value of the rainfall variable,  
364 respectively. The median of these  $N$  values of  $Q_i$  is Sen's estimator of slope. Equation 14 is used  
365 to calculate the Sen's estimator, which ranks the  $N$  values of  $Q_i$  from the smallest to the largest:

$$366 \quad Q_{med} = \begin{cases} Q * \left\lfloor \frac{(N+1)}{2} \right\rfloor, & \text{if } N \text{ is odd} \\ \frac{Q * \left\lfloor \frac{N}{2} \right\rfloor + Q * \left\lfloor \frac{(N+2)}{2} \right\rfloor}{2}, & \text{if } N \text{ is even} \end{cases} \quad (14)$$

367 The sign in Equation 13, indicate the direction of the trend. A time series' trend that is decreasing  
368 or increasing is indicated by a negative or positive value of  $Q_{med}$ , respectively (Mulu et al., 2018).

369

## 370 **2.6 Estimating the impact of climate change on hydrology**

371 To assess the climate change impact on the hydrology of the study catchment, simulations from  
372 four GCM-RCM combinations of climate models were used. Furthermore, for each climate model,  
373 two different RCPs scenarios, i.e., RCP 4.5 and RCP 8.5, were used as inputs to the calibrated  
374 SWAT model to simulate and evaluate the anticipated hydrological variables in the 2030s (2021–  
375 2050) and 2060s (2051–2080) of the century. Simulation results of hydrological variables, namely  
376 precipitation, evapotranspiration, surface runoff, total water yield, lateral, and ground water flow  
377 for the baseline period (1987 to 2016) were compared with the future time periods of the 2030s  
378 and the 2060s simulation. The differences in simulation outputs between the observed baseline  
379 and the future time indicates climate change impacts on the watershed's hydrologic response.

## 380 **3.Results and discussion**

### 381 **3.1 Calibration and validation of SWAT model.**

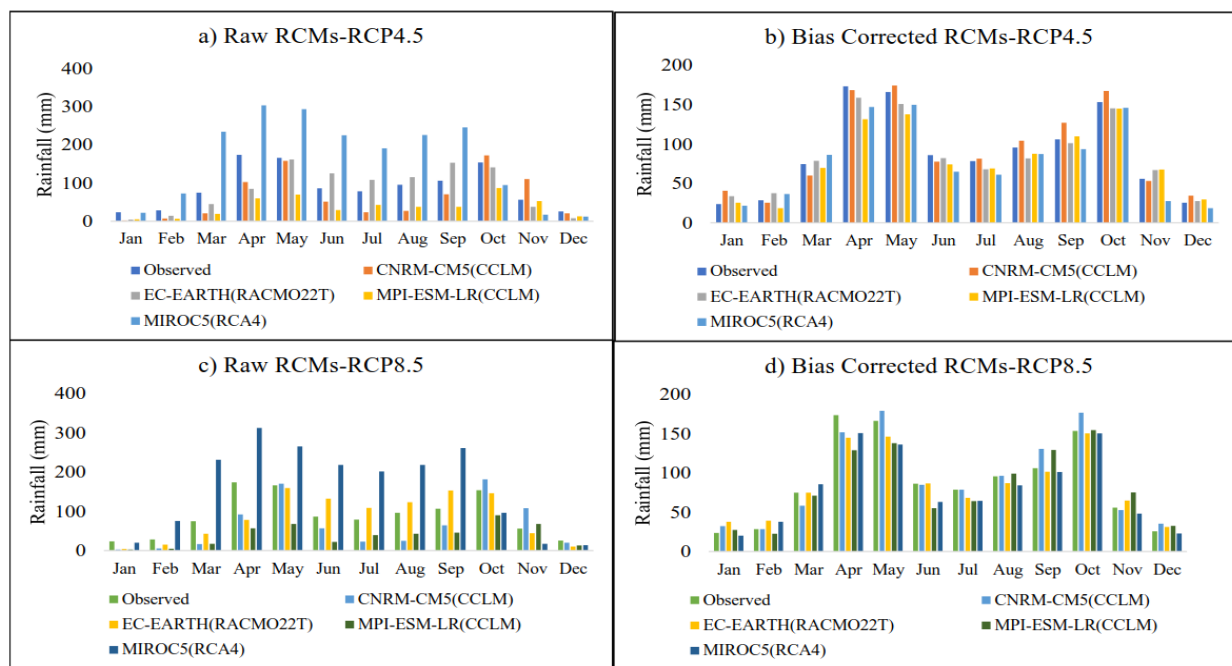
382 The SWAT-CUP software's SUFI-2 algorithms were utilized for sensitivity analysis to identify  
383 key flow parameters influencing streamflow in the SWAT model's calibration and validation.  
384 Initially, twenty-one flow parameters underwent sensitivity analysis, and following that, ten  
385 sensitive flow parameters namely ALPHA\_BF.gw, CN2.mgt, CANMX.hru, GWQMN.gw,  
386 CH\_K2.rte, REVAPMN.gw, SOL\_AWC(..).sol, RCHRG\_DP.gw, ESCO.hru, and  
387 GW\_DELAY.gw, were selected based on p-value (ranging from 0 to 0.5) and t-stat (ranging from  
388 7.86 to 0.65). The details of the analysis presented at Shigute et al. (2022).

389 The SWAT model was calibrated and validated using Chenemassa station's streamflow data from  
390 1987 to 2002 for calibration and from 2003 to 2011 for validation. Results showed good  
391 performance with  $R^2$ , PBIAS, and NSE values of 0.78, -3.2%, and 0.73 during calibration, and  
392 0.74, 3.9%, and 0.72 during validation. Additional information on model calibration, validation,  
393 performance evaluation, and streamflow hydrograph are available in prior studies (e.g., Shigute et  
394 al., 2022)

395

396 **3.2 Bias correction of precipitation and temperature of RCMs**

397 To enhance the forecasting ability of climate models, it is critical to correct the uncertainties and  
 398 discrepancies between the measured and GCM/RCM data, which serve as inputs to the climate  
 399 change impact assessment. For this study, to adjust the overestimation and underestimation of the  
 400 raw output of the RCMs simulations of rainfall and temperature, the linear scaling bias correction  
 401 technique was employed, and the discrepancy of the RCM's simulation of rainfall and temperature  
 402 was adequately corrected with the measured rainfall and temperature data of the study basin.

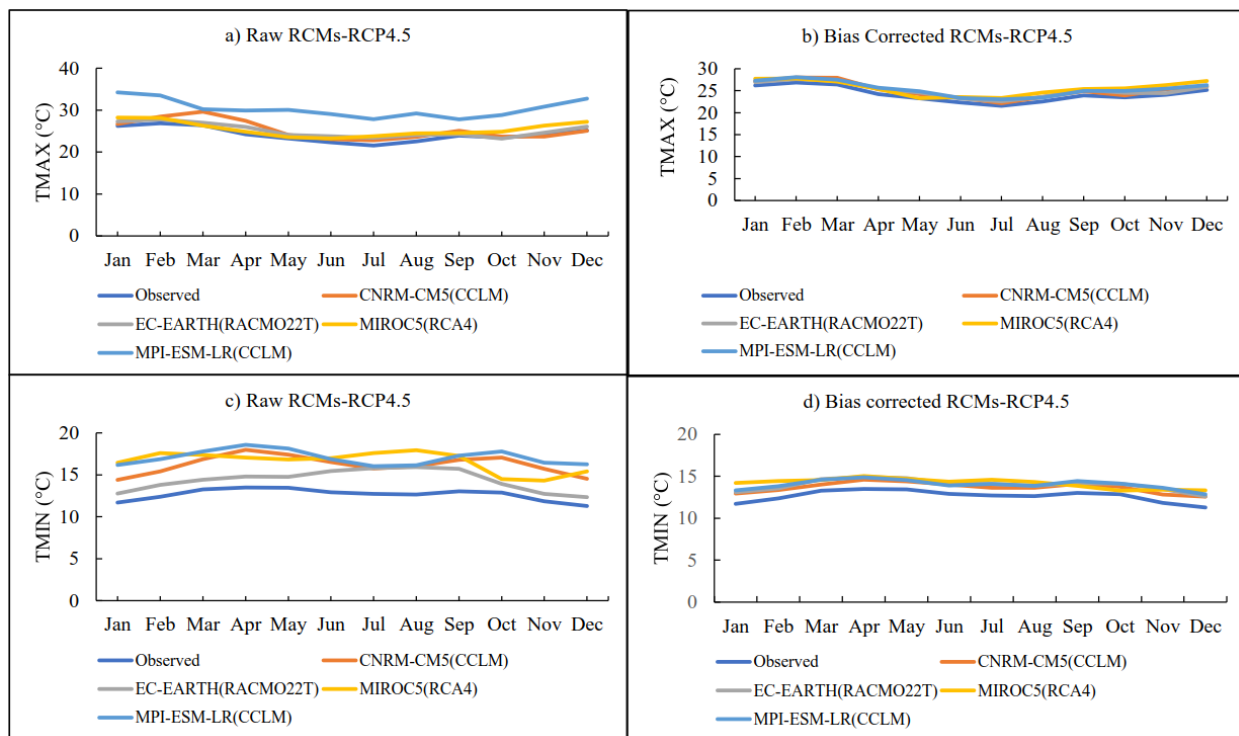


403  
 404 Fig. 2. Performance of RCP 4.5 and RCP8.5 mean rainfall data before and after bias correction. a)  
 405 and c) represent Raw RCM of RCP 4.5 and 8.5 before bias correction and b) and d) RCM of  
 406 RCP4.5 and 8.5 after bias correction.

407 The bias correction procedures effectively corrected the initial overestimation in the raw RCMs  
 408 simulation of monthly rainfall. This was observed from February to September for MIROC5 and  
 409 from June to September for EC-EARTH, as shown in Fig 2a and c. The correction, illustrated in  
 410 Fig 2b and d, significantly improved the discrepancies between the observed and the RCM's  
 411 simulation of average monthly rainfall under RCP 4.5 and RCP 8.5.

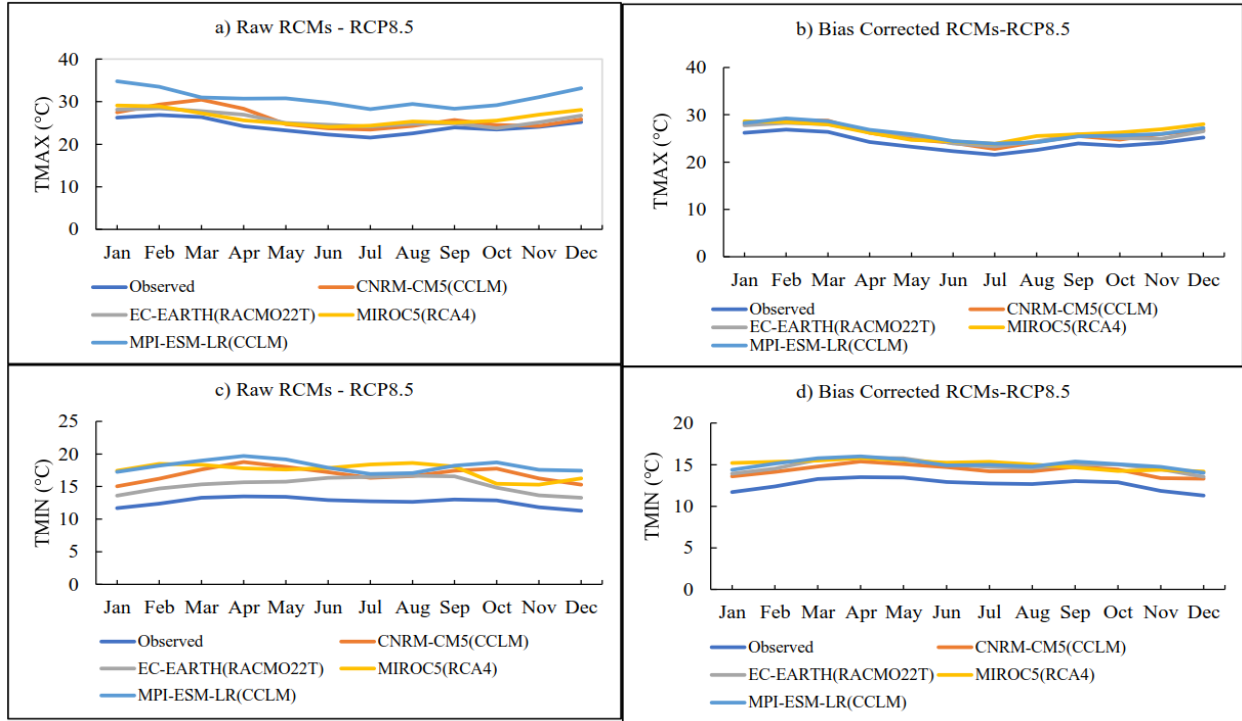
412 Moreover, the initial underestimation in the RCM simulations of CNRM-CM5 and MPI-ESM-LR  
 413 from January to September, and EC-EARTH from January to May, October, and November under

414 RCP 4.5 and 8.5 was successfully addressed. This is also depicted in Fig 2b and d, which also  
 415 show the long-term average monthly rainfall after bias correction for the selected climate models.  
 416 In this regard, the linear scaling method has effectively adjusted both the monthly rainfall  
 417 distribution and the extreme rainfall values.  
 418 Fig. 3 shows that RCMs simulation of RCP 4.5 of TMAX and TMIN appears to be overestimated.  
 419 The overestimation of climate models ranges from 0.22 to 8.01°C for the TMAX and 0.88 to 5.3°C  
 420 for the TMIN during the RCP4.5 scenario (Figs. 3, a and c).



421  
 422 Fig. 3. RCMs simulation of RCP 4.5 monthly average TMAX (°C) and TMIN (°C); raw (a and  
 423 c) and bias corrected (b and d).

424  
 425 In the case of RCP8.5 scenario as shown in Fig. 4 (a and c), the overestimation values of TMAX  
 426 and TMIN range from 0.3 to 8.56°C and from 1.88 up to 6.2°C, respectively.



427

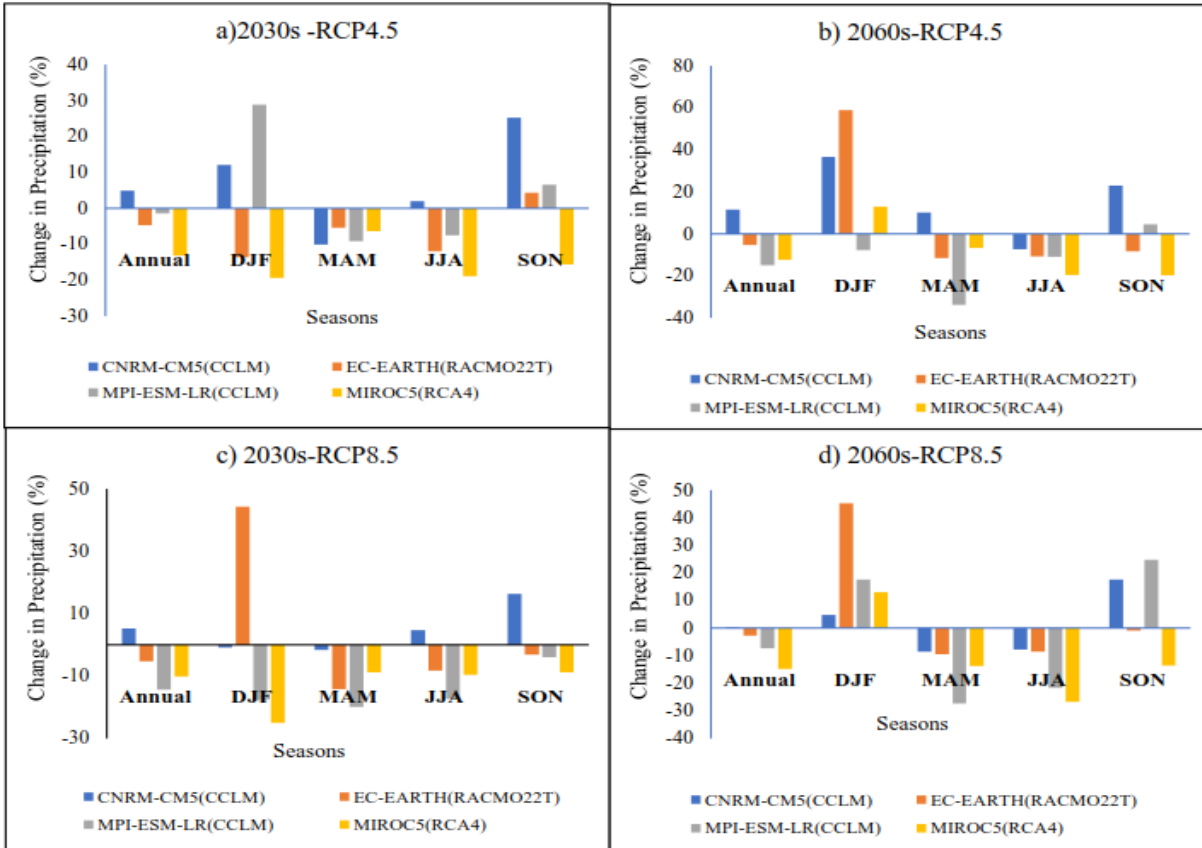
428 Fig. 4. RCMs simulation of RCP 8.5 monthly average TMAX (°C) and TMIN (°C); raw (a and  
 429 c) and bias corrected (b and d).

430 By using bias correction, the RCMs' overestimation of TMAX and TMIN was successfully  
 431 corrected with measured mean monthly TMAX and TMIN. The adjusted TMAX and TMIN the  
 432 climate models after the application of bias correction for RCP4.5 and RCP8.5 is showed on Fig.  
 433 3, (b and d) and Fig. 4, (b and d), respectively.

434 **3.3 Forecasted change in rainfall and temperature**

435 **Future Rainfall Projection**

436 The annual and seasonal change in projected rainfall for the 2030s (2021–2050) and 2060s (2051–  
 437 2080) scenarios for the selected GCM-RCM models for RCP 4.5 and 8.5 emission scenarios are  
 438 presented in Fig. 5.



439

440 Fig. 5. The future annual and seasonal projected change of rainfall of climate models, a) 2030s  
 441 under RCP4.5, b) 2060s under RCP4.5, c) 2030s under RCP8.5, and d) 2060s under RCP8.5.

442 The analysis revealed that future rainfall projections in the study area show a range of magnitudes  
 443 of changes compared to the observed rainfall. For RCP 4.5 and RCP 8.5 emission scenarios, the  
 444 change in annual and seasonal projected rainfall ranges from -33.79 to + 58.95% for the 2030s and  
 445 2060s time periods. In both RCP emission scenarios, during the 2030s and 2060s, the projected  
 446 annual rainfall of the EC-EARTH, MPI-ESM-LR, and MIROC5 models showed likely reductions  
 447 ranging from 1.36 to 14.96%, whereas the CNRM-CM5 model displayed a likely increase ranging  
 448 from 1.43 to 11.6% (Figs. 5 a-d). However, under the RCP 4.5 and RCP 8.5 scenarios, annual  
 449 mean rainfall will likely be reduced by up to 13.1% and 14.36%, respectively, in the 2030s,  
 450 compared to observed rainfall. Similarly, under RCP4.5 and RCP8.5 emission scenarios, during  
 451 the 2060s, annual rainfall is likely to decrease by up to 14.96% and 14.84%, respectively. This  
 452 result is consistent with the findings of other studies conducted in various parts of Ethiopia, which  
 453 reported a likely increase and decrease in future annual rainfall in various parts of Ethiopia (Balcha

454 et al., 2023; Kuma et al., 2021; Takele et al., 2022). For instance, the study undertaken by Takele  
455 et al., (2022) in the upper blue Nile basin showed that during 2030s and 2050s in the two RCPs  
456 scenarios, the projected annual average rainfall is likely to change from -13 to 6%.

457 Under the RCP4.5 emission scenario, the seasonal rainfall projections for DJF, MAM, JJA, and  
458 SON decreased by up to 19.36%, 10.1%, 18.9%, and 15.6%, respectively, during the 2030s (Fig.  
459 5, a). However, in the same future period and scenario (in the 2030s of RCP 4.5), CNRM-CM5  
460 during DJF, JJA, and SON, EC-EARTH during SON, and MPI-ESM-LR during DJF and SON  
461 seasons showed an increasing rainfall (Fig. 5, a). Similarly, in RCP 4.5 scenario, seasonal rainfall  
462 decreased relative to observed rainfall during the 2060s. The reduction of rainfall reached up to  
463 7.65 % during DJF, 33.8% during MAM, 19.6% during JJA, and 19.8% during SON seasons (Fig.  
464 5, b). During the 2030s in RCP 8.5, the seasonal rainfall is anticipated to be reduced by up to 25%,  
465 19%, 17%, and 9% during the DJF, MAM, JJA, and SON seasons, respectively (Fig. 5, C). In the  
466 RCP 8.5 scenario, rainfall in the MAM, JJA, and SON seasons, will likely decrease by up to 27.3%,  
467 26.6%, and 13.5%, respectively, during the 2060s (Fig. 5, d). On the other hand, during the 2030s  
468 of RCP8.5, the CNRM-CM5 climate model in DJF, MAM, and SON seasons, MPI-ESM-LR in  
469 SON, and EC-EARTH and MIROC5 in DJF season, as well as the MPI-ESM-LR, EC-EARTH,  
470 CNRM-CM5, and MIROC5 climate models in the DJF season, and MPI-ESM-LR and CNRM-  
471 CM5 in the SON season in the 2060s of RCP8.5 emission, showed likely increasing rainfall.  
472 During 2030s and 2060s under both RCP scenarios, the change in projected increasing rainfall is  
473 expected to reach up to 58.95%. On the other hand, for the same time periods in both RCP emission  
474 scenarios, most of the evaluated models indicate a decrease in projected rainfall during the MAM  
475 and JJA seasons. This finding agrees with the result of Daniel & Abate (2022) and Kuma et al.  
476 (2021). They found that projected rainfall is expected to increase during DJF and reduce during  
477 the wet seasons of MAM and JJA. In the southern, southeastern, eastern lowland and highland of  
478 Ethiopia, the MAM season used to cultivate crops and agro-pastoral activities (Bekele-Biratu et  
479 al., 2018). A reduction or delay in the MAM and JJA seasons, combined with future temperature  
480 increases, may result in severe drought and a reduction in water resources, posing a threat to  
481 Ethiopia's agricultural development.

482 In general, in the study basin, the annual and seasonal projected rainfall has not shown any  
483 systematic increasing or decreasing trend. This indicates that climate models do not agree on the

484 magnitude and direction of future changes in annual and seasonal rainfall amounts for future time  
 485 periods. These variations in forecasting future changes are most probably a result of the use of  
 486 different climate models and subsequent parameterizations (Bekele et al., 2021).

### 487 **Future Temperature Projection**

488 The expected changes in maximum and minimum temperatures of the selected climate models for  
 489 the RCP 4.5 and RCP 8.5 scenarios for the 2030s and 2060s are summarized in Table 3. The result  
 490 displayed that during the 2030s, in the RCP 4.5 scenario, minimum and maximum temperatures  
 491 are expected to rise up to 1.3°C and 1.2°C, respectively. During the 2060s, in this same emission  
 492 scenario, the minimum and maximum temperatures would increase to 1.82°C and 1.74°C,  
 493 respectively. Similarly, during 2030s in RCP 8.5 scenarios, the minimum and maximum  
 494 temperature is expected to rise up to 1.6°C and 1.36°C, respectively. During 2060s in RCP 8.5  
 495 scenario, the minimum and maximum temperature may raise up to 3.02°C and 2.85°C,  
 496 respectively. The analysis result also displayed that the change in temperature during 2060s  
 497 expected to be higher than 2030s in both the RCPs. Furthermore, in both RCP scenarios, during  
 498 2030s and 2060s, the rate of change in minimum temperature would be higher than the maximum  
 499 temperature.

500 Table 3. Future mean annual minimum and maximum temperatures change under both RCP  
 501 scenarios.

GCM - RCM	2030s (2021-2050)				2060s (2051-2080)			
	RCP 4.5		RCP 8.5		RCP 4.5		RCP 8.5	
	TMAX (°C)	TMIN (°C)	TMAX (°C)	TMIN (°C)	TMAX (°C)	TMIN (°C)	TMAX (°C)	TMIN (°C)
CNRM-CM5(CCLM)	0.61	0.65	0.89	0.87	1.22	1.28	2.18	2.09
EC-EARTH(RACMO22T)	0.67	0.98	0.78	1.19	1.38	1.73	2.19	2.77
MIROC5(RCA4)	1.2	1.3	1.36	1.59	1.7	1.82	2.85	2.91
MPI-ESM-LR(CCLM)	0.76	1.04	1.26	1.31	1.74	1.78	2.52	3.02
Average	0.81	0.99	1.07	1.24	1.51	1.65	2.44	2.7

502  
 503 In general, the analysis results revealed that under the RCP 8.5 scenario, the expected change in  
 504 the minimum and maximum temperatures of the individual and average climate models would be  
 505 higher than the RCP 4.5 scenario. This is because RCP8.5 has a higher emission scenario than  
 506 RCP4.5. Furthermore, the results of all climate and average models showed that the change in

507 minimum temperature would be more significant than the change in maximum temperature in both  
508 the 2030s and 2060s. This finding is consistent with the results (Bekele et al., 2019; Bekele et al.,  
509 2021; Moges & Bhat, 2021; Takele et al., 2022; Tessema et al., 2021; Worku et al., 2021). They  
510 showed that the expected change in minimum and maximum temperature is higher in RCP 8.5  
511 than RCP 4.5. Furthermore, they found that the increase in minimum temperature were higher than  
512 the increase in maximum temperature in different parts of Ethiopia.

### 513 **3.4. Analysis of future annual and seasonal rainfall trends**

514 The annual and seasonal projected rainfall trend analysis results are displayed in Table 4. The MK  
515 trend test in the RCP 4.5 and RCP 8.5 emission scenarios revealed both positive and negative  
516 trends for annual and seasonal rainfall in the 2030s and 2060s, indicating the existence of variations  
517 in climate models for predicting climate in terms of magnitude and direction. The decreasing and  
518 increasing trends in all RCMs and future time periods (2030s and 2060s) under the two RCP  
519 scenarios range from 0.05 to 7.43mm per year and 0.03 to 7.01mm per year, respectively. During  
520 the 2030s in RCP 4.5 and RCP 8.5, the MK test for MAM and annual future rainfall data indicated  
521 an insignificant trend, but it showed a decreasing tendency with rates ranging from 0.97 to 6.16  
522 mm per year for the MPI-ESM-LR, EC-EARTH, and CNRM-CM5 climate models. However, the  
523 RCP 8.5 of the 2060s of the RCM of MIROC5 and MPI-ESM-LR model showed statistically  
524 significant increasing and decreasing trend at 95% confidence level, with a rate of 3.34 and 7.43  
525 mm per year, respectively. On the other hand, most of the RCMs showed an insignificant  
526 increasing trend during the JJA season. However, the detected trends were significant for EC-  
527 EARTH of the RCP 8.5 in the 2030s. During the SON season, most RCMs show a decreasing  
528 trend, with rates ranging from 0.27 to 3.62 mm per year in the 2030s and 2060s scenarios.

529

530

531

532

533

534

535 Table 4. Trends of seasonal and annual projected rainfall under RCP4.5 and RCP8.5

GCM-RCM	RCPs	Periods	DJF		MAM		JJA		SON		Annual-RF	
			P-value	Sen's slope	P-value	Sen's slope	P-value	Sen's slope	P-value	Sen's slope	P-value	Sen's slope
CNRM-CM5 (CCLM)	RCP4.5	2030s	0.38	0.58	0.24	-3.53	1.00	0.00	0.97	-0.27	0.92	-0.97
		2060s	0.60	-0.82	0.70	1.88	0.08	3.77	0.78	-1.37	1.00	0.03
	RCP8.5	2030s	0.70	0.32	0.09	-5.22	0.17	2.16	0.97	0.11	0.55	-4.60
		2060s	0.94	-0.12	0.34	2.16	0.21	2.49	0.44	2.89	0.17	7.01
EC-EARTH (RACMO22T)	RCP4.5	2030s	1.00	-0.07	0.06	-4.11	0.83	-0.11	0.70	0.69	0.36	-3.17
		2060s	0.67	0.75	0.42	1.46	0.97	-0.06	0.11	-2.27	0.83	-0.64
	RCP8.5	2030s	0.75	0.52	0.06	-3.99	<b>0.03*</b>	1.41	0.09	-2.17	0.19	-3.96
		2060s	0.80	0.29	0.48	1.59	0.27	-0.86	0.09	2.76	0.11	4.40
MIROC5 (RCA4)	RCP4.5	2030s	0.26	1.20	0.55	1.19	0.57	0.50	<b>0.04*</b>	2.04	0.08	3.99
		2060s	0.97	0.11	1.00	0.07	0.94	0.22	0.08	-1.92	0.80	-1.14
	RCP8.5	2030s	0.23	0.94	0.67	0.59	0.65	-0.39	0.50	1.72	1.00	-0.05
		2060s	0.86	-0.32	<b>0.01*</b>	3.34	0.72	0.35	0.19	1.82	0.10	4.86
MPI-ESM-LR (CCLM)	RCP4.5	2030s	0.19	1.56	0.27	-5.43	0.40	1.50	0.40	-3.62	0.44	-5.13
		2060s	0.60	-0.32	0.60	1.36	0.80	-0.53	0.80	-1.63	0.92	-0.28
	RCP8.5	2030s	0.50	0.42	0.21	-3.67	0.97	0.24	0.50	-2.16	0.32	-6.16
		2060s	0.80	0.31	<b>0.048*</b>	-7.43	0.14	2.96	0.65	2.53	0.75	-2.70
Ensemble Mean	RCP4.5	2030s	0.17	1.31	0.11	-2.80	0.44	0.68	0.67	-0.65	0.50	-1.84
		2060s	0.48	0.38	0.27	2.00	0.36	0.86	0.19	-1.65	0.97	-0.12
	RCP8.5	2030s	0.21	0.95	0.17	-2.59	0.21	0.80	0.50	-0.62	0.38	-2.67
		2060s	0.94	0.10	0.55	-1.14	0.06	1.62	0.08	3.01	0.48	2.17

536 DJF is from December to February, MAM is from March to May, JJA is from June to August, and SON is from  
 537 September to November; \* Indicate significance at  $\alpha = 0.05$ .  
 538

539  
 540 The mean seasonal and annual projected rainfall trends analysis in Table 4 indicated that the annual  
 541 rainfall projection in both RCPs showed an insignificant decreasing trend during the 2030s and  
 542 2060s. Similarly, except for the 2060s of RCP 4.5 and RCP 8.5, the MAM and SON seasons  
 543 displayed a decreasing trend. On the contrary, DJF and JJA seasons during the 2030s and 2060s  
 544 in both RCPs, as well as RCP 4.5 of the 2060s of MAM and RCP 8.5 of the 2060s of SON, showed  
 545 a positive trend.

546 **3.5 Seasonal and annual projected temperature trend.**

547 The annual, seasonal, and an ensemble mean of maximum and minimum temperature trends for  
 548 2030s and 2060s under RCP 4.5 and RCP 8.5 emission scenarios are presented in Tables 5 and 6.  
 549 During the 2030s and 2060s in the RCP 4.5 scenario, the MK analysis result of the seasonal and  
 550 annual minimum and maximum temperatures exhibited an increasing trend. However, during the

551 2030s in the RCP 4.5 scenario, most of the seasonal and annual maximum and minimum  
552 temperatures of the RCM of the MPI-ESM-LR, CNRM-CM5, and EC-EARTH showed a  
553 significantly increasing trend at 1% and 5% levels of confidence. On a seasonal basis, during the  
554 2030s in the RCP4.5, climate model of CNRM-CM5 (in MAM, JJA, and SON), EC-EARTH (in  
555 DJF, MAM, JJA, and SON), MPI-ESM-LR (in MAM, SON, and JJA), and MIROC5 (in DJF and  
556 JJA) seasons showed statistically significant increasing trend at 1% and 5% level of confidence.  
557 Similarly, the annual and seasonal ensemble means of minimum and maximum temperatures  
558 during the 2030s and 2060s in RCP4.5 emission showed a significant increasing trend at the 1%  
559 and 5% levels of confidence.

560 Table 6 displays projected temperature trends for RCP8.5 in the 2030s and 2060s for all RCM  
561 models. The trend results show that there is an increasing trend in seasonal, annual, and ensemble  
562 mean minimum and maximum temperatures. Specifically, most of the seasons in the CNRM-CM5  
563 and EC-EARTH models show a significant increase in seasonal temperatures at 1% and 5%  
564 confidence levels. Additionally, the ensemble mean of maximum and minimum temperatures in  
565 the 2030s and 2060s, as well as the MPI-ESM-LR and MIROC5 models in the 2060s under  
566 RCP8.5, exhibit statistically significant trends at both 1% and 5% confidence levels.

567 The Sen's slope of seasonal and annual temperature in the future periods under both the RCPs  
568 emission scenarios are summarized in Table 5 and Table 6. Accordingly, during 2030s and 2060s  
569 in both RCPs, the annual, seasonal and an ensemble mean of the slope of change of minimum  
570 temperature was higher than the slope of change of the annual, seasonal and an ensemble mean  
571 maximum temperature in most of RCMs model. The rate of slope change in minimum temperature  
572 during the 2030s and 2060s forecast period varies from 0.004°C to 0.059°C per annual, whereas  
573 in case of maximum temperature, the rate of slope changes varies from -0.007°C to 0.61°C per  
574 annual. On the other hand, the rate of slope of change varies from 0.003 to 0.071°C for minimum  
575 temperature and from 0.004°C to 0.096°C for the maximum temperature in the 2030s and 2060s  
576 of the RCP8.5 emission scenario. This finding is in line with a study by Takele et al. (2022) in the  
577 Upper Blue Nile basin and Worku et al. (2021) in the Jemma sub-basin. They found out that, in  
578 the near and long term of 21st century most of the evaluated RCM models showed statistically  
579 significant increasing trend of maximum and minimum temperature at 1% and 5% significance  
580 level. In addition, they discovered that the rate of slope change in the minimum temperature is

581 higher than that of maximum temperature. According to the IPCC report, anthropogenic forcing  
582 are likely to have contributed significantly to surface temperature increases across all continents  
583 (IPCC., 2014).

584 In general, the observed potential increase in maximum and minimum temperature in the 2030s  
585 and 2060s in the two RCP scenarios during the MAM, JJA, and SON seasons may result in dryer  
586 conditions at the start of the rainy season, increasing the rate of evapotranspiration and delaying  
587 the onset of rainy seasons in the area. This has a significant impact on rainfed agriculture practices,  
588 particularly for crops with longer growing seasons. Furthermore, due to decreased water supply  
589 and increased water demands, irrigation water requirements are likely to increase, potentially  
590 reducing crop yield. Future temperature increases in the study watershed could have an impact on  
591 the hydrologic cycle, water resource system, hydropower, and water use.

592

593

594

595

596

597

598

599

600

601

602

603

604

605 Table 5. Summary of trends in seasonal and annual projected maximum and minimum temperature under RCP4.5.

GCM-RCM	RCP-4.5	Parameters	DJF		MAM		JJA		SON		Annual	
			Tmax(°C)	Tmin (°C)	Tmax(°C)	Tmin (°C)	Tmax(°C)	Tmin (°C)	Tmax(°C)	Tmin (°C)	Tmax(°C)	Tmin (°C)
CNRM-CM5 (CCLM)	2030s	P-Value	0.457	0.087	0.087	<b>0.008**</b>	<b>0.02*</b>	<b>0.0007**</b>	0.214	<b>0.001**</b>	<b>0.007**</b>	<b>&lt; 0.0001**</b>
		Sen's slope	0.008	0.028	0.031	0.019	0.04	0.027	0.014	0.026	0.023	0.027
	2060s	P-Value	<b>0.037*</b>	0.101	0.166	0.101	0.888	0.058	0.101	0.242	<b>0.026*</b>	<b>0.012*</b>
		Sen's slope	0.028	0.023	0.036	0.021	-0.004	0.02	0.034	0.009	0.024	0.016
EC-EARTH (RACMO22T)	2030s	P-Value	0.288	<b>0.0001**</b>	<b>0.024*</b>	<b>0.016*</b>	0.094	<b>0.0001**</b>	0.832	<b>0.019*</b>	0.009	<b>0.0003**</b>
		Sen's slope	0.015	0.046	0.045	0.019	0.019	0.029	0.003	0.017	0.02	0.023
	2060s	P-Value	0.646	<b>0.004**</b>	0.832	0.272	0.416	0.256	0.069	0.081	0.054	<b>0.006**</b>
		Sen's slope	0.009	0.035	-0.005	0.007	0.013	0.01	0.024	0.008	0.016	0.017
MIROC5 (RCA4)	2030s	P-Value	<b>0.041*</b>	0.117	0.805	0.724	0.081	<b>0.012*</b>	0.548	0.189	0.480	0.075
		Sen's slope	0.028	0.059	-0.007	0.006	0.036	0.024	0.01	0.022	0.009	0.03
	2060s	P-Value	0.087	0.256	0.888	0.646	0.750	0.117	0.166	0.256	0.166	0.135
		Sen's slope	0.026	0.028	0.001	0.006	0.007	0.018	0.023	0.026	0.017	0.022
MPI-ESM-LR (CCLM)	2030s	P-Value	0.069	0.075	<b>0.035*</b>	<b>0.03*</b>	0.177	<b>0.029*</b>	<b>0.004**</b>	0.135	<b>0.004**</b>	<b>0.0065**</b>
		Sen's slope	0.027	0.031	0.041	0.046	0.035	0.029	0.061	0.022	0.045	0.024
	2060s	P-Value	0.646	0.087	0.339	0.075	0.457	0.724	0.502	0.214	0.972	0.069
		Sen's slope	0.009	0.023	0.017	0.017	-0.019	0.004	0.014	0.015	0.0008	0.016
Ensemble Mean	2030s	P-Value	<b>0.0037**</b>	<b>0.00045**</b>	<b>0.0084**</b>	<b>0.0073**</b>	<b>0.037*</b>	<b>&lt; 0.0001**</b>	<b>0.0042**</b>	<b>0.0004**</b>	<b>0.0073**</b>	<b>0.00068**</b>
		Sen's slope	0.021	0.043	0.033	0.020	0.021	0.023	0.027	0.019	0.018	0.019
	2060s	P-Value	<b>0.00043**</b>	<b>0.001**</b>	0.304	<b>0.02*</b>	0.860	<b>0.016*</b>	<b>0.011*</b>	<b>0.026**</b>	<b>0.024*</b>	<b>0.019*</b>
		Sen's slope	0.023	0.030	0.014	0.014	0.002	0.015	0.021	0.013	0.014	0.016

606

607 DJF is from December to February, MAM is from March to May, JJA is from June to August, and SON is from September to November; \*\* and \* show significance  
608 at  $\alpha = 0.01$  and  $0.05$ , respectively

609 Table 6. Summary of trends in seasonal and annual projected maximum and minimum temperature under RCP8.5.

GCM-RCM	RCP-8.5	Parameters	DJF		MAM		JJA		SON		Annual	
			Tmax(°C)	Tmin (°C)	Tmax(°C)	Tmin (°C)	Tmax(°C)	Tmin (°C)	Tmax(°C)	Tmin (°C)	Tmax(°C)	Tmin (°C)
CNRM-CM5 (CCLM)	2030s	P-Value	<b>0.004**</b>	<b>0.049*</b>	<b>0.001**</b>	<b>0.022*</b>	<b>0.0002**</b>	<b>0.0002**</b>	<b>0.0075**</b>	<b>&lt; 0.0001**</b>	<b>0.0013**</b>	<b>0.0017**</b>
		Sen's slope	0.031	0.036	0.063	0.024	0.021	0.034	0.043	0.031	0.037	0.033
	2060s	P-Value	<b>0.0003**</b>	<b>0.0037**</b>	<b>0.012*</b>	<b>&lt; 0.0001**</b>	<b>&lt; 0.0001**</b>	<b>&lt; 0.0001**</b>	<b>0.008**</b>	<b>0.0003**</b>	<b>&lt; 0.0001**</b>	<b>&lt; 0.0001**</b>
		Sen's slope	0.051	0.06	0.053	0.066	0.049	0.061	0.033	0.031	0.061	0.071
EC-EARTH (RACMO22T)	2030s	P-Value	0.109	<b>0.0005**</b>	<b>0.0002**</b>	<b>&lt; 0.0001**</b>	<b>0.0047**</b>	<b>&lt; 0.0001**</b>	<b>0.0075**</b>	<b>&lt; 0.0001**</b>	<b>&lt; 0.0004**</b>	<b>&lt; 0.0001**</b>
		Sen's slope	0.026	0.049	0.036	0.042	0.04	0.051	0.041	0.045	0.042	0.030
	2060s	P-Value	0.081	<b>&lt; 0.0001**</b>	<b>0.016*</b>	<b>&lt; 0.0001**</b>	<b>0.0003**</b>	<b>&lt; 0.0001**</b>	0.109	<b>&lt; 0.0001**</b>	<b>&lt; 0.0001**</b>	<b>&lt; 0.0001**</b>
		Sen's slope	0.032	0.056	0.047	0.054	0.06	0.056	0.03	0.041	0.041	0.05
MIROC5 (RCA4)	2030s	P-Value	<b>0.024*</b>	0.054	0.621	0.256	0.321	<b>0.018*</b>	0.081	0.832	0.075	<b>0.038*</b>
		Sen's slope	0.033	0.054	0.004	0.016	0.022	0.028	0.023	0.003	0.02	0.03
	2060s	P-Value	<b>0.0002**</b>	<b>0.012*</b>	0.101	<b>0.01**</b>	0.155	0.069	<b>0.038*</b>	0.77	<b>0.0006**</b>	<b>0.0008**</b>
		Sen's slope	0.059	0.054	0.028	0.029	0.031	0.016	0.04	0.070	0.041	0.039
MPI-ESM-LR (CCLM)	2030s	P-Value	<b>0.0053**</b>	<b>0.004**</b>	0.256	0.081	0.457	0.201	<b>0.026*</b>	<b>0.008**</b>	<b>0.013*</b>	<b>0.016*</b>
		Sen's slope	0.032	0.053	0.021	0.028	0.010	0.01	0.039	0.026	0.026	0.023
	2060s	P-Value	<b>0.0023**</b>	<b>0.0002**</b>	<b>&lt; 0.0001</b>	<b>0.0003**</b>	0.28	<b>0.028*</b>	<b>0.0075**</b>	<b>&lt; 0.0001**</b>	<b>0.0032**</b>	<b>&lt; 0.0001**</b>
		Sen's slope	0.049	0.06	0.096	0.064	0.033	0.030	0.05	0.065	0.029	0.056
Ensemble Mean	2030s	P-Value	<b>&lt; 0.0001**</b>	<b>&lt; 0.0001**</b>	<b>&lt; 0.0001**</b>	<b>&lt; 0.0001**</b>	<b>&lt; 0.0001**</b>	<b>&lt; 0.0001**</b>	<b>&lt; 0.0001**</b>	<b>0.0001**</b>	<b>&lt; 0.0001**</b>	<b>&lt; 0.0001**</b>
		Sen's slope	0.028	0.050	0.034	0.035	0.041	0.046	0.035	0.021	0.03	0.034
	2060s	P-Value	<b>&lt; 0.0001**</b>	<b>&lt; 0.0001**</b>	<b>&lt; 0.0001**</b>	<b>&lt; 0.0001**</b>	<b>0.0006**</b>	<b>&lt; 0.0001**</b>	<b>0.0001**</b>	<b>&lt; 0.0012**</b>	<b>&lt; 0.0001**</b>	<b>&lt; 0.0001**</b>
		Sen's slope	0.049	0.063	0.048	0.053	0.037	0.037	0.04	0.018	0.037	0.046

610  
611 DJF is from December to February, MAM is from March to May, JJA is from June to August, and SON is from September to November; \*\* and \* show significance  
612 at  $\alpha = 0.01$  and  $0.05$ , respectively

### 613 3.6. Climate change impact on the hydrological processes

614 To forecast the potential impacts of climate change on the hydrological components under RCP4.5  
615 and RCP8.5 scenarios, future rainfall and temperature in the 2030s (2021–2050) and 2060s (2051–  
616 2080) periods and a previously calibrated and validated SWAT model, were used. The simulated  
617 hydrological response of the base period (1987-2016) and the future periods (2030s and 2060s)  
618 were then compared to evaluate the change in the watershed's future hydrological components.

619 The result of the impact of future climate change on the hydrological components based on the  
620 simulated precipitation, total water yield, surface runoff, ET, groundwater flow, and lateral flow  
621 of the SWAT models is presented in Table 7. The result displayed that, during 2030s and 2060s  
622 under RCP 4.5 and RCP 8.5 scenario, the surface runoff changes from -33.47% to 24.47% and -  
623 39.3% to 5.29%, respectively. The highest increment of surface runoff, which is 24.47%, was  
624 observed during 2060s under RCP4.5 scenario. In contrast, the highest reduction of surface runoff,  
625 which is 39.03% was observed during 2030s under RCP8.5 scenario. The climate model of MPI-  
626 ESM-LR and CNRM-CM5 showed the highest negative and positive change in surface runoff,  
627 respectively. In addition to this, Table 7 showed that, except for the CNRM-CM climate model,  
628 all the models show a likely decrease in surface runoff in the future periods in both RCP scenarios.

629 Furthermore, the analysis results indicate that, under the two Representative Concentration  
630 Pathways (RCPs), the anticipated hydrological components, specifically surface runoff, water  
631 yield, lateral flow, and groundwater flow, are expected to experience significant decreases in the  
632 2030s and 2060s. The projected reductions are estimated to reach up to 39.3%, 39.8%, 40.08%,  
633 and 50.06%, respectively, in comparison to the 1987–2016 base period for all climate models  
634 except the CNRM-CM5. Under CNRM -CM5 model, annual runoff, total water yield, ground  
635 waterflow, lateral flow, and are likely to increase by up to 24.47%, 28.56%, 27.98%, and 23.26%,  
636 respectively. However, during the 2030s and 2060s under the two RCPs, the annual ET may  
637 increase across the basin in all climate model. The rise in ET is triggered mainly by a consistent  
638 rise in temperature. The expected change in increase of annual ET varies from 0.94% to 8.11% in  
639 all scenarios. The reduction or increase of future annual total water yield, runoff, lateral, and  
640 ground waterflow associated with the decrease or increase of future periods simulated precipitation  
641 in the study basin. For instance, a 2.88% increase in mean annual rainfall during 2030s under  
642 RCP4.5 scenario resulted in an increasing surface runoff, ground waterflow, lateral flow, and total

643 water yield by 8.78%, 4.32%, 7.67%, and 9.17% for the CNRM-CM5 model. On the other hand,  
644 a 15.8% reduction of annual average rainfall during 2060s under RCP8.5 for MIRCOS models  
645 will lead to 31.89%, 27.68%, 40.59%, and 29.37% reduction of total water yield, runoff, ground  
646 waterflow, and lateral flow, respectively. This study's findings are consistent with those of other  
647 studies conducted in Ethiopia (Daniel & Abate, 2022; Merga et al., 2022; Takele et al., 2022;  
648 Worku et al., 2021). For example, a study conducted by Worku et al. (2021) in the Jemma sub-  
649 basin, Ethiopia, showed that under RCP4.5 and RCP8.5 scenarios, the impact of climate change  
650 may result in reduced runoff, water yield, groundwater, lateral flow, and an increase in  
651 evapotranspiration during the near- and long-term (2021–2050 and 2071–2100) periods.

652 In general, decreasing surface water under the scenarios will have a significant impact on  
653 agricultural activities. Reductions in rainfall along with increasing temperatures are expected to  
654 have a significant effect on the main economic sectors, such as agriculture and water resource  
655 sectors, of the study watershed. Moreover, the dominant rain-fed, non-input-intensive way of  
656 agricultural practices, together with the economic dependency of most people's livelihoods on  
657 agriculture production, make the area susceptible to climate change and variability (MoWE,  
658 2007b; Shigute et al., 2023) If extreme weather events and the effects of climate change continue  
659 in the future, subsistence and smallholder farmers' vulnerability may worsen, triggering further  
660 economic loss (Miheretu, 2020).

661

662

663

664

665

666

667 Table 7. Baseline and future climate models' mean annual water balance components under RCP4.5 and RCP8.5.

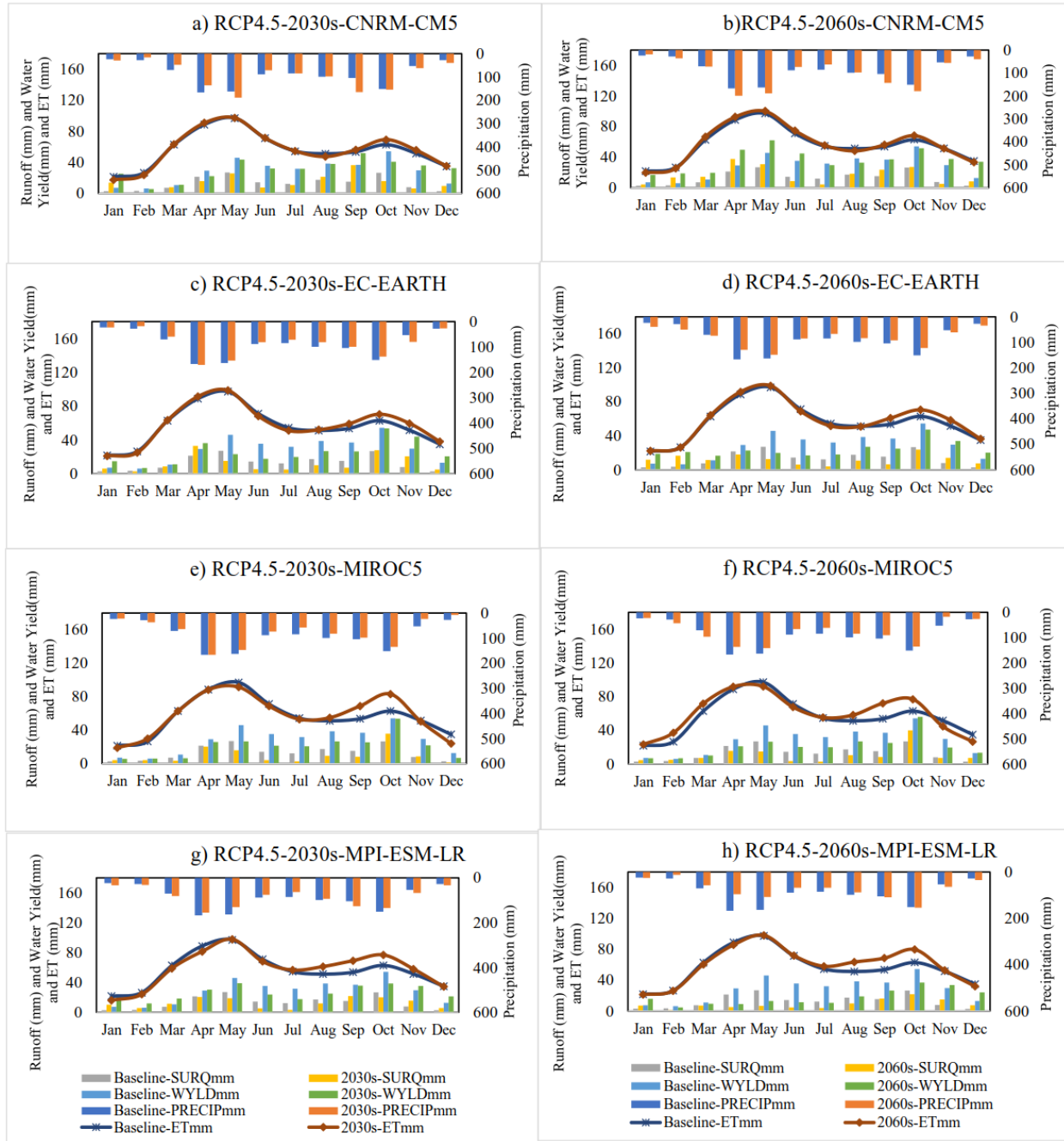
GCM-RCM	RCP	Period	PRECIPmm	% Change	ETmm	% Change	SURQmm	% Change	GW_Qmm	% Change	LAT_Qmm	% Change	WYLDmm	% Change
	Baseline	1987-2016	1060.25		676.76		159.03		141.31		37.92		339.63	
CNRM-CM5 (CCLM)	RCP4.5	2030s	1090.74	2.88	683.13	0.94	173.00	8.78	147.42	4.32	40.83	7.67	370.77	9.17
		2060s	1164.48	9.83	692.26	2.29	197.95	24.47	180.85	27.98	46.74	23.26	436.63	28.56
	RCP8.5	2030s	1089.72	2.78	698.44	3.20	167.44	5.29	148.21	4.88	40.42	6.58	365.37	7.58
		2060s	1049.61	-1.00	706.95	4.46	156.47	-1.61	133.66	-5.42	37.28	-1.70	336.15	-1.03
EC-EARTH (RACMO22T)	RCP4.5	2030s	1001.41	-5.55	698.05	3.15	147.14	-7.48	116.95	-17.24	31.56	-16.78	301.88	-11.12
		2060s	988.26	-6.79	700.59	3.52	142.65	-10.30	107.89	-23.65	29.83	-21.34	286.08	-15.77
	RCP8.5	2030s	991.32	-6.50	702.86	3.86	146.35	-7.97	113.40	-19.75	31.15	-17.86	297.64	-12.36
		2060s	1019.60	-3.83	708.63	4.71	150.13	-5.60	123.82	-12.38	31.99	-15.64	313.16	-7.80
MIROC5 (RCA4)	RCP4.5	2030s	915.47	-13.66	695.19	2.72	119.16	-25.07	95.35	-32.53	27.35	-27.88	248.07	-26.96
		2060s	923.87	-12.86	716.79	5.92	125.89	-20.84	92.78	-34.34	27.17	-28.36	251.99	-25.80
	RCP8.5	2030s	946.86	-10.69	706.87	4.45	124.90	-21.46	107.19	-24.15	28.14	-25.81	267.16	-21.34
		2060s	892.47	-15.82	726.40	7.33	115.01	-27.68	83.95	-40.59	26.79	-29.37	231.33	-31.89
MPI-ESM-LR (CCLM)	RCP4.5	2030s	1026.19	-3.21	703.16	3.90	151.62	-4.66	124.80	-11.69	33.61	-11.37	318.32	-6.27
		2060s	881.71	-16.84	717.53	6.02	105.81	-33.47	76.71	-45.72	26.85	-29.20	214.86	-36.74
	RCP8.5	2030s	877.02	-17.28	710.29	4.95	96.53	-39.30	70.57	-50.06	22.73	-40.08	204.47	-39.80
		2060s	956.51	-9.78	731.62	8.11	128.75	-19.04	104.16	-26.29	30.06	-20.73	278.57	-17.98

668

669 PRECIPmm, Precipitation in millimeter; ETmm, Evapotranspiration in millimeter; SURQmm, Surface runoff in millimeter; GW\_Qmm, Ground waterflow in  
670 millimeter; LAT\_Qmm, Lateral flow in millimeter; WYLDmm, Total water yield in millimeter.

671

672



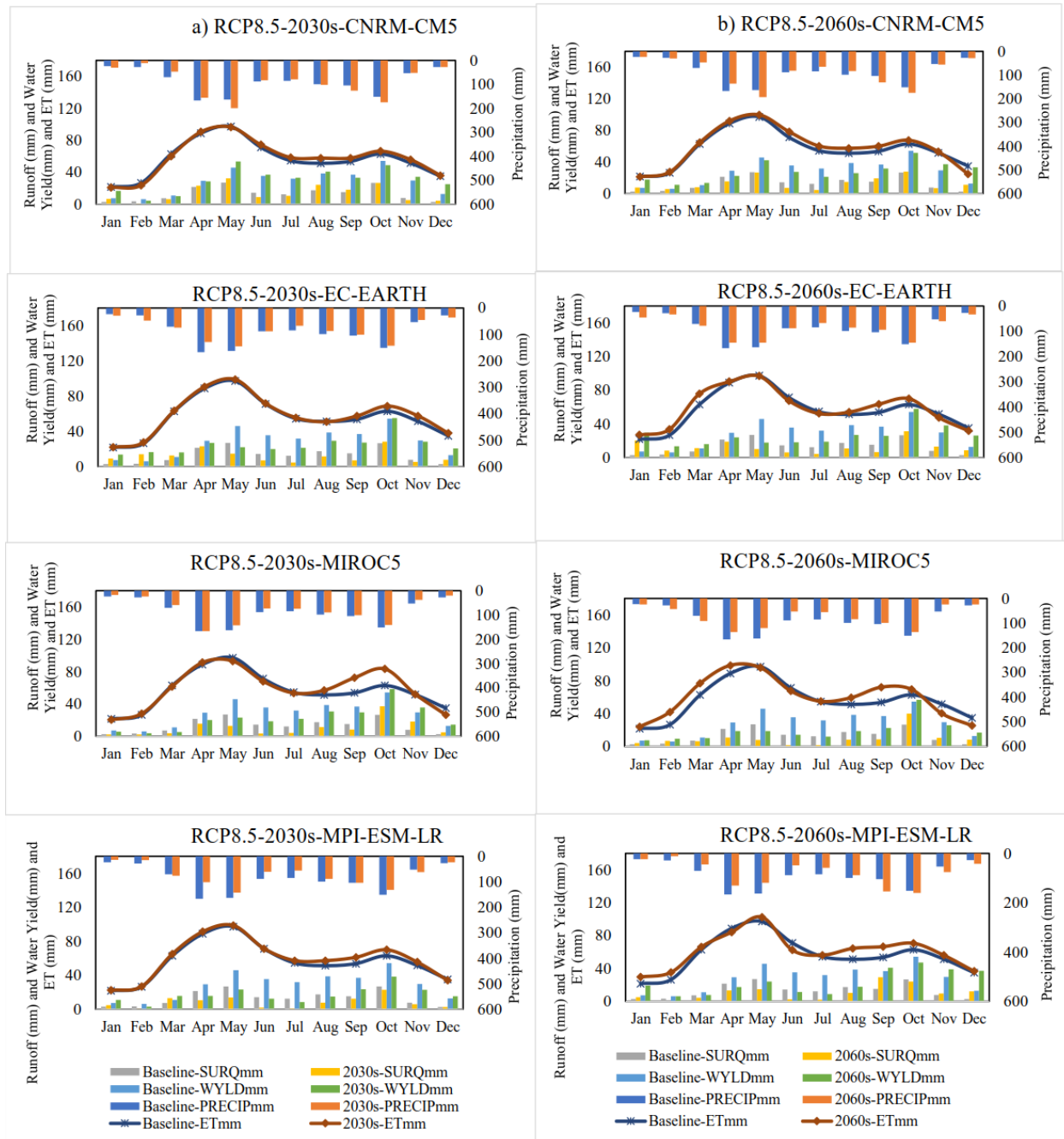
673

674 Fig. 6. Represent the average monthly simulated precipitation, evapotranspiration, surface runoff,  
 675 and water yield for different climate models and time periods (2030s and 2060s) under RCP4.5  
 676 scenario. Models include CNRM-CM5, EC-EARTH, MIROC5, and MPI-ESM-LR.

677 The simulated mean monthly hydrological components of the baseline and the future climate  
 678 model under the two RCPs during 2030s and 2060s in the Fig. 6 and 7 a-h shows that highest value  
 679 of average monthly water yield, runoff, and ET were observed during the spring (MAM) and

680 autumn (SON) seasons. Furthermore, except the CNRM-CM5 model, during 2030s and 2060s  
681 under RCP4.5, the climate models EC-EARTH, MIROC5, and MPI-ESM-LR showed likely  
682 reduction of water yield and surface runoff in most months from April to October (Fig. 6 c-h).  
683 Similarly, Fig. 7 (a - h) during the future period under RCP8.5, in most month from April to  
684 September for EC-EARTH, March to September for MIROC5, and March to October for MPI-  
685 ESM-LR climate models reduction of water yield and surface runoff is anticipated. During the  
686 future time (2030s and 2060s) under the two RCP, from March to August up to 68% runoff and  
687 57% water yield reduction expected for EC-EARTH model. Similarly, for MIROC5 up to 62% of  
688 water yield and 88% surface runoff and for MPI-ESM-LR up to 72% of water yield and 86%  
689 surface runoff reduction is anticipated. The result for MPI-ESM-LR, MIROC5, and EC-EARTH  
690 models also showed that the simulated rainfall in most months from March to October, is likely to  
691 be reduced during the 2030s and 2060s under the two emission scenarios. In contrast to other  
692 hydrological parameters such as runoff, water yield, groundwater flow, and lateral flow,  
693 evapotranspiration is expected to increase in all climate models during most months in the 2030s  
694 and 2060s under the two emission scenarios. This is due to an increasing future temperature in all  
695 climate models. The likely reduction of total water yield and runoff in the future period may be  
696 due to reduction of rainfall, increasing of temperature and increasing of evapotranspiration in the  
697 study basin. Different research in different parts of Ethiopia stated that reduction of hydrological  
698 parameters mainly total water yield, surface runoff, and ground waterflow linked with an  
699 increasing of evapotranspiration and temperature and reduction of rainfall (Daniel & Abate, 2022;  
700 Takele et al., 2022; Tessema et al., 2021; Worku et al., 2021).

701



702

703 Fig. 7. Shows mean monthly simulated precipitation, surface runoff, water yield and  
 704 evapotranspiration for different climate models (i.e., CNRM-CM5, EC-EARTH, MIROC5, and  
 705 MPI-ESM-LR) and time periods (2030s and 2060s) under RCP8.5 scenario.

706

707

708 Overall, the impact of climate change due to an increasing temperature and a reduction of rainfall  
709 that is likely to occur in the future time under the RCP4.5 and RCP8.5 scenarios significantly affect  
710 the water resource of the upper Genale River basin. The likely reduction of runoff, ground  
711 waterflow, lateral flow, and total water yield as well as an increase of ET in the study basin may  
712 result in a water stress. Water stress, especially due to the reduction of total water yield, runoff,  
713 and groundwater flow during the rainy season may cause extensive impact on water supply for  
714 domestic and livestock, agricultural activities, and ecosystem service in the study basin. A change  
715 in rainfall and temperature could have significantly reduced agricultural yield and, in the worst  
716 cases, causes complete crop failure, leading to famine and deaths of both humans and animal  
717 (Shigute et al., 2023). Therefore, to deal with the expected negative effects of climate change on  
718 agricultural development and other sectors due to future warming of temperature and decrease of  
719 rainfall amount and distribution, it is essential to design and implement watershed management  
720 practices, develop management and adaptation measure, and water allocation system in the study  
721 basin.

## 722 **Summary and conclusion**

723 Climate change affects the water resource of the river basin. To assess the likely impacts of climate  
724 change on the hydrological components and water resource potential of the upper Genale River  
725 basin during 2030s and 2060s under RCP4.5 and RCP8.5, bias corrected future temperature and  
726 precipitation data from CORDEX Africa RCMs (EC-EARTH, CNRM-CM5, MIROC5, and MPI-  
727 ESM-LR) were applied in to calibrated SWAT model.

728 The result shows that except for the CNRM-CM5 climate model, the predicted climate shows a  
729 rise in temperature and a decrease in rainfall in all future times (in the 2030s and 2060s) under the  
730 two RCPs. The change in future temperature and rainfall in comparison with the baseline period  
731 could significantly affect the hydrological components. Under both RCPs, rising temperatures and  
732 decreasing precipitation during the 2030s and 2060s are projected to significantly reduce the  
733 annual hydrological components of the entire study basin. Total water yield, runoff, ground  
734 waterflow, and lateral flow are all expected to decline within a range of 1.03% to 39.8%, 1.61%  
735 to 39%, 5.42% to 50%, and 1.7% to 40.1%, respectively. However, evapotranspiration is projected  
736 to increase significantly in these future scenarios. The observed change in hydrological parameters  
737 such as reduction of water yield, runoff, lateral flow, ground waterflow flow as well as a rise in

738 evapotranspiration in the study watershed evidently associated with the future change in  
739 temperature and rainfall. The reduction of water resources, especially during the rainy seasons can  
740 cause extensive impact on agriculture and ecosystem service of the basin.

741 The declining of runoff, total water yield, and ground waterflow along with an increasing  
742 evapotranspiration due to future impact of climate change has boarder implication for developing  
743 and managing water resource. In this regard, designing and implementing water resource  
744 management strategies is indispensable for minimizing the potential impact of climate change on  
745 water resources in the study basin. To develop an efficient and long-lasting water resource  
746 management strategy in the watershed, it is critical to incorporate projected and simulated climate  
747 and hydrologic variables into adaptation decision analysis. In line with this, it is crucial to  
748 implement policies and strategies that enhance the water resource systems in the study basin in  
749 order to increase the capacity for dealing with the anticipated impact of climate change and  
750 variability on hydrological variables. An increase in climate change related research and designing  
751 and implementing effective water resource management strategies to provide optimal benefits to  
752 adapt and mitigate the impact of climate change and maintaining the water resources availability,  
753 would be one approach.

754 As a result, the current research has provided valuable insight into the expected rainfall and  
755 temperature trends, as well as the future impact of climate change on hydrological elements in the  
756 study basin, which is essential for managing water resources and maintaining sustainable  
757 agricultural production. As a result, the results of this study contribute to a better understanding of  
758 the available water resource potential, as well as to water resource planning, management, and  
759 development for current and future development projects in the study basin. Moreover, the study's  
760 findings and methodology can be used to develop guidelines for other regions and the Genale  
761 Dawa River basin in the future. To further enhance the results, we propose additional research in  
762 the study watershed that provides more detailed and accurate information for modeling work that  
763 takes into account high-quality climatic data, different climate models as well as different bias  
764 correction approaches, the use of different hydrologic models, and the combined effect of  
765 socioeconomic, climate, and land use change in the study watershed.

766

767

768 **ACKNOWLEDGEMENTS**

769 We would like to express our gratitude to the Ethiopian Ministry of Water and Energy, as well as  
770 the Ethiopian Meteorological Service Agency, for offering streamflow and meteorological data for  
771 the study area. Dr. Christopher E. Ndehedehe is supported by funding from the Australian  
772 Research Council (DE230101327).

773 **AUTHORS' CONTRIBUTIONS**

774 Authors' contributions: **Mehari Shigute:** Writing – original draft, Writing – review & editing,  
775 Methodology, Formal analysis, Conceptualization, Investigation, Software. **Tena Alamirew:**  
776 Supervision, Conceptualization, Investigation. **Adane Abebe:** Conceptualization, Supervision.  
777 **Christopher E. Ndehedehe:** Writing – original draft, Writing – review & editing. **Habtamu**  
778 **Tilahun Kassahun:** Conceptualization, Writing – original draft.

779 **AVAILABILITY OF DATA AND MATERIAL:**

780 All data generated or analyzed during this study are included and available in this article and can  
781 be available from the authors on reasonable request.

782 **DECLARATIONS**

783 **FUNDING**

784 This work was supported by Addis Ababa University and Dilla University and Australian Rivers  
785 Institute, Griffith University, Brisbane.

786 **Ethics approval and consent to participate** Not applicable

787 **CONFLICT OF INTEREST**

788 The authors declare no conflict of interest.

789 **References**

790 Abbaspour, K. C. (2015). *SWAT-CUP: SWAT calibration and uncertainty programs—a user*  
791 *manual*. Eawag: Dübendorf, Switzerland, 16-70.

792 Abbaspour, K. C., Vaghefi, S. A., & Srinivasan, R. (2018). A Guideline for Successful  
793 Calibration and Uncertainty Analysis for Soil and Water Assessment : A Review of Papers  
794 from the 2016 International SWAT Conference. *Water*, 10(6).

- 795 <https://doi.org/10.3390/w10010006>
- 796 Abera, K., & Gebeyehu, A. (2023). Hydrological drought forecasting and monitoring system  
797 development using artificial neural network ( ANN ) in Ethiopia. *Heliyon*, 9(2), e13287.  
798 <https://doi.org/10.1016/j.heliyon.2023.e13287>
- 799 Abeysingha, N. S., Islam, A., & Singh, M. (2020). *Assessment of climate change impact on flow*  
800 *regimes over the Gomti River basin under IPCC AR5 climate change scenarios*. 303–326.  
801 <https://doi.org/10.2166/wcc.2018.039>
- 802 Abraham, & Nadew. (2018). Impact of Land Use Land Cover Dynamics on Water Balance ,  
803 Lake Ziway Watershed, Ethiopia. *Hydrology: Current Research*, 9(4), 309.
- 804 Adera, A. G., & Alfredsen, K. T. (2020). *Climate change and hydrological analysis of Tekeze*  
805 *river basin Ethiopia : implication for potential hydropower production*. 744–759.  
806 <https://doi.org/10.2166/wcc.2019.203>
- 807 Adugna, M., Boru, N., & Debele, A. (2021). Impact of climate change on potential  
808 evapotranspiration and crop water requirement in Upper Wabe Bridge watershed , Wabe  
809 Shebele River. *Journal of African Earth Sciences*, 180(2021), 104223.  
810 <https://doi.org/10.1016/j.jafrearsci.2021.104223>
- 811 Akoko, G., Le, T. H., Gomi, T., & Kato, T. (2021). A Review of SWAT Model Application in  
812 Africa. *Water*, 13(9), 1313. <https://doi.org/10.3390/w13091313>
- 813 Alemayehu, A., & Bewket, W. (2017). Local spatiotemporal variability and trends in rainfall and  
814 temperature in the central highlands of Ethiopia. *Geografiska Annaler, Series A: Physical*  
815 *Geography*, 99(2), 85–101. <https://doi.org/10.1080/04353676.2017.1289460>
- 816 Alexandersson, H. (1986). A homogeneity test applied to precipitation data. *Journal of*  
817 *Climatology*, 6(6), 661–675. <https://doi.org/10.1002/joc.3370060607>
- 818 Arnold, J. G., & Fohrer, N. (2005). SWAT2000 : Current Capabilities and Research  
819 Opportunities in Applied watershed Modelling. *Hydrological Processes*, 19, 563–572.  
820 <https://doi.org/10.1002/hyp.5611>
- 821 Arnold, J. G., Moriasi, D. N., Gassman, P. W., Abbaspour, K. C., White, M. J., Srinivasan, R.,  
822 Santhi, C., Harmel, R. D., Griensven, A. Van, Van Liew, M. W., Kannan, N., & Jha, M. K.  
823 (2012). SWAT: Model Use, Calibration, and Validation. *Transactions of the American*  
824 *Society of Agricultural and Biological Engineers*, 55(4), 1491–1508.
- 825 Arnold, J. G., Srinivasan, R., Muttiah, R. S., & Williams, J. R. (1998). Large area hydrologic  
826 modeling and assessment: Part I. Model development. *Journal of the American Water*  
827 *Resources Association*, 34(1), 73–89.
- 828 Asfaw, A., Simane, B., Hassen, A., & Bantider, A. (2018). Variability and time series trend  
829 analysis of rainfall and temperature in northcentral Ethiopia: A case study in Woleka sub-  
830 basin. *Weather and Climate Extremes*, 19(2018), 29–41.  
831 <https://doi.org/10.1016/j.wace.2017.12.002>
- 832 Awotwi, A., Annor, T., Anornu, G. K., Quaye-Ballard, J. A., Agyekum, J., Ampadu, B., Nti, I.  
833 K., Gyampo, M. A., & Boakye, E. (2021). Climate change impact on streamflow in a

- 834 tropical basin of Ghana, West Africa. *Journal of Hydrology: Regional Studies*,  
835 34(September 2020), 100805. <https://doi.org/10.1016/j.ejrh.2021.100805>
- 836 Awulachew, S. B., Yilma, A. D., Loiskandl, W., Ayana, M., & Alamirew, T. (2007). Water  
837 resources and irrigation development in Ethiopia. Colombo, Sri Lanka: International Water  
838 Management Institute (IWMI) 66p. In [*IWMI Working Paper 123*].
- 839 Azman, A. H., Tukimat, N. N. A., & Malek, M. A. (2022). Analysis of Linear Scaling Method in  
840 Downscaling Precipitation and Temperature. *Water Resources Management*, 36(1), 171–  
841 179. <https://doi.org/10.1007/s11269-021-03020-0>
- 842 Balcha, S. K., Awass, A. A., Hulluka, T. A., Bantider, A., & Ayele, G. T. (2023). Assessment of  
843 future climate change impact on water balance components in Central Rift Valley Lakes  
844 Basin, Ethiopia. *Journal of Water and Climate Change*, 14(1), 175–199.  
845 <https://doi.org/10.2166/wcc.2022.249>
- 846 Bekele-Biratu, E., Thiaw, W. M., & Korecha, D. (2018). Sub-seasonal variability of the Belg  
847 rains in Ethiopia. *International Journal of Climatology*, 38(7), 2940–2953.  
848 <https://doi.org/10.1002/joc.5474>
- 849 Bekele, D., Alamirew, T., Kebede, A., Zeleke, G., Assefa, M., & Bekele, D. (2021). Modeling  
850 the impacts of land use and land cover dynamics on hydrological processes of the Keleta  
851 watershed , Ethiopia. *Sustainable Environment*, 7(1), 0–14.  
852 <https://doi.org/10.1080/27658511.2021.1947632>
- 853 Bekele, D., Alamirew, T., Kebede, A., Zeleke, G., & Melesse, A. M. (2019). Modeling Climate  
854 Change Impact on the Hydrology of Keleta Watershed in the Awash River Basin , Ethiopia.  
855 *Environmental Modeling & Assessment*, 24, 95–107. 10.1007/s10666-018-9619-1
- 856 Bekele, W. T., Haile, A. T., & Rientjes, T. (2021). Impact of Climate Change on the Streamflow  
857 of the Arjo-Didessa catchment Under RCP Scenarios. *Journal of Water and Climate  
858 Change*, 1–13. <https://doi.org/10.2166/wcc.2021.307>
- 859 Belihu, M., Tekleab, S., Abate, B., & Bewket, W. (2020). Hydrologic response to land use land  
860 cover change in the Upper Gidabo Watershed, Rift Valley Lakes Basin, Ethiopia.  
861 *HydroResearch*, 3, 85–94. <https://doi.org/10.1016/j.hydres.2020.07.001>
- 862 Bewket, W., Radeny, M., & Mungai, C. (2015). Agricultural Adaptation and Institutional  
863 Responses to Climate Change Vulnerability in Ethiopia. *CCAFS Working Paper No. 106*.  
864 *CGIAR Research Program on Climate Change, Agriculture and Food Security (CCAFS)*.  
865 *Copenhagen, Denmark*. [www.ccafs.cgiar.org](http://www.ccafs.cgiar.org)
- 866 Birkinshaw, S. J., Guerreiro, S. B., Nicholson, A., Liang, Q., Quinn, P., Zhang, L., He, B., Yin,  
867 J., & Fowler, H. J. (2017). Climate change impacts on Yangtze River discharge at the Three  
868 Gorges Dam. *Hydrology and Earth System Sciences*, 21(4), 1911–1927.  
869 <https://doi.org/10.5194/hess-21-1911-2017>
- 870 Bizuneh, B. B., Moges, M. A., Sinshaw, B. G., & Kerebih, M. S. (2021). SWAT and HBV  
871 models ' response to streamflow estimation in the upper Blue Nile Basin , Ethiopia. *Water-  
872 Energy Nexus*, 4, 41–53. <https://doi.org/10.1016/j.wen.2021.03.001>
- 873 Bogale, S. (2021). Hydrological Response to Land Use and Land Cover Changes of Ribb

- 874 Watershed , Ethiopia. *Hydrology*, 9(1), 1–12. <https://doi.org/10.11648/j.hyd.20210901.11>
- 875 Buishand, T. . (1982). Some Methods for Testing the Homogeneity of Rainfall Records. *Journal*  
876 *of Hydrology*, 58(1–2), 11–27. [https://doi.org/doi:10.1016/0022-1694\(82\)90066-x](https://doi.org/doi:10.1016/0022-1694(82)90066-x)
- 877 Chaemiso, S. E., Abebe, A., & Pingale, S. M. (2016). Assessment of the impact of climate  
878 change on surface hydrological processes using SWAT: a case study of Omo-Gibe river  
879 basin, Ethiopia. *Modeling Earth Systems and Environment*, 2(4), 1–15.  
880 <https://doi.org/10.1007/s40808-016-0257-9>
- 881 Chimdessa, K., Quraishi, S., Kebede, A., & Alamirew, T. (2019). Effect of land use land cover  
882 and climate change on river flow and soil loss in Didessa River Basin, South West Blue  
883 Nile, Ethiopia. *Hydrology*, 6(2), 1–20. <https://doi.org/10.3390/hydrology6010002>
- 884 Daba, M. H., & You, S. (2020). Assessment of climate change impacts on river flow regimes in  
885 the upstream of awash basin, ethiopia: Based on ipcc fifth assessment report (ar5) climate  
886 change scenarios. *Hydrology*, 7(4), 1–22. <https://doi.org/10.3390/hydrology7040098>
- 887 Daniel, H., & Abate, B. (2022). Effect of climate change on stream fl ow in the Gelana  
888 watershed , Rift valley basin, Ethiopia. *Journal of Water & Climate Change*, 13(5), 2205–  
889 2232. <https://doi.org/10.2166/wcc.2022.059>
- 890 Dariane, A. B., & Pouryafar, E. (2021). Quantifying and projection of the relative impacts of  
891 climate change and direct human activities on streamflow fluctuations. *Climatic Change*  
892 (2021), 165(34). <https://doi.org/10.1007/s10584-021-03060-w>
- 893 Degefu, M. A., Tadesse, Y., & Bewket, W. (2021). Observed changes in rainfall amount and  
894 extreme events in southeastern Ethiopia, 1955–2015. *Theoretical and Applied Climatology*,  
895 144(3–4), 967–983. <https://doi.org/10.1007/s00704-021-03573-5>
- 896 Dibaba, W. T., Demissie, T. A., & Miegel, K. (2020). Watershed Hydrological Response to  
897 Combined Land Use / Land Cover and Climate Change in Highland Ethiopia: Finchaa  
898 Catchment. *Water*, 12(4), 1801. <https://doi.org/doi:10.3390/w12061801>
- 899 Dibaba, W. T., Miegel, K., & Demissie, T. A. (2019). Evaluation of the CORDEX regional  
900 climate models performance in simulating climate conditions of two catchments in Upper  
901 Blue Nile Basin. *Dynamics of Atmospheres and Oceans*, 87(August), 101104.  
902 <https://doi.org/10.1016/j.dynatmoce.2019.101104>
- 903 Dinku, T., Cousin, R., Corral, J., Ceccato, P., Thomson, M. C., Faniriantsoa, R., Khomyakov, I.,  
904 & Vardillo, A. (2016). The ENACTS Approach: Transforming climate services in Africa  
905 one country at a time. *World Policy Papers*, 1–24.
- 906 Dinku, T., Hailemariam, K., Maidment, R., Tarnavsky, E., & Connor, S. (2014). Combined use  
907 of satellite estimates and rain gauge observations to generate high-quality historical rainfall  
908 time series over Ethiopia. *International Journal of Climatology*, 34(7), 2489–2504.  
909 <https://doi.org/10.1002/joc.3855>
- 910 Dosio, A., Lennard, C., & Spinoni, J. (2022). Projections of indices of daily temperature and  
911 precipitation based on bias - adjusted CORDEX - Africa regional climate model  
912 simulations. *Climatic Change*, 1–24. <https://doi.org/10.1007/s10584-022-03307-0>

- 913 Eisner, S., Flörke, M., Chamorro, A., Daggupati, P., Donnelly, C., Huang, J., Hundecha, Y.,  
 914 Koch, H., Kalugin, A., Krylenko, I., Mishra, V., Piniewski, M., Samaniego, L., Seidou, O.,  
 915 Wallner, M., & Krysanova, V. (2017). An ensemble analysis of climate change impacts on  
 916 streamflow seasonality across 11 large river basins. *Climatic Change*, 141(3), 401–417.  
 917 <https://doi.org/10.1007/s10584-016-1844-5>
- 918 Emiru, N. C., Recha, J. W., Thompson, J. R., Belay, A., Aynekulu, E., Manyevere, A., Demissie,  
 919 T. D., Osano, P. M., Hussein, J., Molla, M. B., Mengistu, G. M., & Solomon, D. (2022).  
 920 Impact of Climate Change on the Hydrology of the Upper Awash River Basin , Ethiopia.  
 921 *Hydrology*, 9, 3. <https://doi.org/10.3390/hydrology9010003>
- 922 EPCC. (2015). Ethiopian Panel on Climate Change: First Assessment Report, Working Group  
 923 II Biodiversity and Ecosystems. *Ethiopian Academy of Sciences. Addis Ababa, Ethiopia.*
- 924 Eromo, S., Adane, C., Santosh, A., & Pingale, M. (2016). Assessment of the impact of climate  
 925 change on surface hydrological processes using SWAT : a case study of Omo-Gibe river  
 926 basin , Ethiopia. *Modeling Earth Systems and Environment*, 2(4), 1–15.  
 927 <https://doi.org/10.1007/s40808-016-0257-9>
- 928 Galata, A. W., Tullu, K. T., & Guder, A. C. (2021). Evaluating watershed hydrological responses  
 929 to climate changes at Hangar Watershed, Ethiopia. *Journal of Water and Climate Change*,  
 930 12(6), 2271–2287. <https://doi.org/10.2166/wcc.2021.229>
- 931 Girvetz, E., Ramirez-Villegas, J., Claessens, L., Lamanna, C., Navaroo-Racines, C., Nowak, A.,  
 932 & Thornton, P. (2019). *Future climate projections in Africa: where are we headed?. in The*  
 933 *Climate-Smart Agriculture Papers* (T. S. Rosenstock, A. Nowak, & E. Girvetz (eds.)).  
 934 Springer, Cham. <https://doi.org/10.1007/978-3-319-92798-5>
- 935 Godfrey, S., & Tunhuma, F. A. (2020). The Climate Crisis: Climate Change Impacts, trend and  
 936 Vulnerabilities of Children inSub Sahara Africa. *United Nations Children’s Fund and*  
 937 *Esatern and Southern Africa Regional Office. Nairobi*, 1–72.  
 938 <https://doi.org/10.2307/j.ctvmd85w3.12>
- 939 Hamed, K. H. (2009). Enhancing the effectiveness of prewhitening in trend analysis of  
 940 hydrologic data. *Journal of Hydrology*, 368(1–4), 143–155.
- 941 Hargreaves, G. H., & Samani, Z. A. (1985). Reference crop evapotranspiration from  
 942 temperature. *Applied Engineering in Agriculture*, 1(2), 96–99.  
 943 <https://doi.org/10.13031/2013.26773>
- 944 Hussain, M., Liu, G., Yousaf, B., Ahmed, R., Uzma, F., Ali, M. U., Ullah, H., & Butt, A. R.  
 945 (2018). Regional and sectoral assessment on climate-change in Pakistan: Social norms and  
 946 indigenous perceptions on climate-change adaptation and mitigation in relation to global  
 947 context. *Journal of Cleaner Production*, 200, 791–808.  
 948 <https://doi.org/10.1016/j.jclepro.2018.07.272>
- 949 IPCC. (2014). *Synthesis Report. Contribution of Working Groups I, II and III to the Fifth*  
 950 *Assessment Report of the Intergovernmental Panel on Climate Chang [Core Writing Team,*  
 951 *R.K. Pachauri and L.A. Meyer (eds.)].IPCC, Geneva, Switzerland, 151 pp.*  
 952 <https://www.ipcc.ch/report/ar5/syr/>

- 953 IPCC. (2013). *T. F. Stocker, D. Qin, G. K. Plattner, M. Tignor, S. K. Allen, J. Boschung, A.*  
 954 *Nauels, Y. Xia, V. Bex & P. M. Midgley (Eds.). Climate Change 2013 The Physical Science*  
 955 *Basis. Cambridge University Press.*
- 956 Kendall, M. G. (1975). *Rank Correlation Methods* (4th ed.). Charles Griffin, London.
- 957 Ketema, A., & Dwarakish, G. S. (2021). Hydro-meteorological impact assessment of climate  
 958 change on Tikur Wuha watershed in Ethiopia. *Sustainable Water Resources Management,*  
 959 *7(4), 1–20.* <https://doi.org/10.1007/s40899-021-00547-3>
- 960 Kuma, H. G., Feyessa, F. F., & Demissie, T. A. (2021). Hydrologic responses to climate and  
 961 land-use / land-cover changes in the Bilate. *Journal of Water & Climate Change, 12(8),*  
 962 *3750–3769.* <https://doi.org/10.2166/wcc.2021.281>
- 963 Lotfirad, M., Adib, A., Salehpoor, J., Ashrafzadeh, A., & Kisi, O. (2021). Simulation of the  
 964 impact of climate change on runoff and drought in an arid and semiarid basin (the  
 965 Hablehroud, Iran). *Applied Water Science, 11(10), 1–24.* <https://doi.org/10.1007/s13201-021-01494-2>
- 967 Luo, M., Liu, T., & Meng, F. (2018). Comparing Bias Correction Methods Used in Downscaling  
 968 Precipitation and Temperature from Regional Climate Models : A Case Study from the  
 969 Kaidu River Basin in Western China. *Water, 10(1046).* <https://doi.org/10.3390/w10081046>
- 970 Mahmood, R., & Babel, M. S. (2013). Evaluation of SDSM developed by annual and monthly  
 971 sub-models for downscaling temperature and precipitation in the Jhelum basin, Pakistan and  
 972 India. *Theoretical and Applied Climatology, 113(1–2), 27–44.*  
 973 <https://doi.org/10.1007/s00704-012-0765-0>
- 974 Mahmood, R., & Jia, S. (2017). An extended linear scaling method for downscaling temperature  
 975 and its implication in the Jhelum River basin, Pakistan, and India, using CMIP5 GCMs.  
 976 *Theoretical and Applied Climatology, 130(3–4), 725–734.* <https://doi.org/10.1007/s00704-016-1918-3>
- 978 Mahmood, R., Jia, S., Tripathi, N. K., & Shrestha, S. (2018). Precipitation extended linear  
 979 scaling method for correcting GCM precipitation and its evaluation and implication in the  
 980 transboundary Jhelum River basin. *Atmosphere, 9(5).* <https://doi.org/10.3390/atmos9050160>
- 981 Mann, H. B. (1945). Nonparametric Tests Against Trend. *Econometrica, 13(3), 245–259.*  
 982 <https://doi.org/10.2307/1907187>
- 983 Mengistu, D., Bewket, W., Dosio, A., & Panitz, H. (2020). Climate change impacts on water  
 984 resources in the Upper Blue Nile (Abay) River Basin, Ethiopia. *Journal of Hydrology.*  
 985 <https://doi.org/10.1016/j.jhydrol.2020.125614>
- 986 Merga, D. D., Adeba, D., Regasa, M. S., & Leta, M. K. (2022). Evaluation of Surface Water  
 987 Resource Availability under the Impact of Climate Change in the Dhidhessa Sub-Basin ,  
 988 Ethiopia. *Atmosphere, 13,* 1296. <https://doi.org/10.3390/atmos13081296> Academic
- 989 Miheretu, B. A. (2020). Temporal variability and trend analysis of temperature and rainfall in the  
 990 Northern highlands of Ethiopia. *Physical Geography, 00(00), 1–18.*  
 991 <https://doi.org/10.1080/02723646.2020.1806674>

- 992 Moges, D. M., & Bhat, H. G. (2021). Climate change and its implications for rainfed agriculture  
 993 in Ethiopia. *Journal of Water and Climate Change*, 12(4), 1229–1244.  
 994 <https://doi.org/10.2166/wcc.2020.058>
- 995 Moriasi, D. N., Arnold, J. G., Liew, M. W. Van, Bingner, R. L., Harmel, R. D., & Veith, T. L.  
 996 (2007). Model evaluation guidelines for systematic quantification of accuracy in watershed  
 997 simulations. *Transactions of the American Society of Agricultural and Biological*  
 998 *Engineers*, 50(3), 885–900.
- 999 MoWE. (2007a). *Genale-Dawa River Basin Integrated Resources Development Master Plan*  
 1000 *Study, Sector Report; Volume II, A. Hydrology and Climate; Lahmeyer International*  
 1001 *GmbH, Germany in association with Yeshi-Ber Consult: Addis Ababa, Ethiopia Addis*  
 1002 *Ababa, Ethiopia.*
- 1003 MoWE. (2007b). *Genale-Dawa River Basin Integrated Resources Development Master Plan*  
 1004 *Study, Sector Report; Volume II, K. Crop Production; Lahmeyer International GmbH,*  
 1005 *Germany in association with Yeshi-Ber Consult: Addis Ababa, Ethiopia.*
- 1006 Mulu, A., Fasnamol, T. M., & Dwarakish, G. S. (2018). *Estimation of Changes in Annual Peak*  
 1007 *Flows in Netravathi River Basin, Karnataka, India BT - Climate Change Impacts* (V. P.  
 1008 Singh, S. Yadav, & R. N. Yadava (eds.); pp. 193–199). Springer Singapore.
- 1009 Musie, M., Sen, S., & Srivastava, P. (2020). Application of CORDEX-AFRICA and NEX-  
 1010 GDDP datasets for hydrologic projections under climate change in Lake Ziway sub- basin ,  
 1011 Ethiopia. *Journal of Hydrology: Regional Studies*, 31, 100721.  
 1012 <https://doi.org/10.1016/j.ejrh.2020.100721>
- 1013 Narsimlu, B., Gosain, A. K., & Chahar, B. R. (2015). SWAT Model Calibration and Uncertainty  
 1014 Analysis for Streamflow Prediction in the Kunwari River Basin , India , Using Sequential  
 1015 Uncertainty Fitting. *Environmental Process*, 2(1), 79–95. [https://doi.org/10.1007/s40710-](https://doi.org/10.1007/s40710-015-0064-8)  
 1016 [015-0064-8](https://doi.org/10.1007/s40710-015-0064-8)
- 1017 Näschen, K., Diekkrüger, B., Leemhuis, C., Seregina, L. S., & van der Linden, R. (2019). Impact  
 1018 of climate change on water resources in the Kilombero Catchment in Tanzania. *Water*  
 1019 *(Switzerland)*, 11(4). <https://doi.org/10.3390/w11040859>
- 1020 Nash, J., & Sutcliffe, J. (1970). River flow forecasting through conceptual models: part I—a  
 1021 discussion of principles. *Journal of Hydrology*, 10, 282–290.
- 1022 Nasiri, S., Ansari, H., & Ziaei, A. N. (2020). Simulation of water balance equation components  
 1023 using SWAT model in Samalqan Watershed (Iran). *Arabian Journal of Geosciences*,  
 1024 13(11). <https://doi.org/10.1007/s12517-020-05366-y>
- 1025 Neitsch, S. L., Arnold, J. G., Kiniry, J. R., & Willians, J. R. (2011). *Soil & Water Assessment*  
 1026 *Tool Theoretical Documentation Version 2009. Texas Water Resources Institute. Texas*  
 1027 *AgriLife Research and USDA Agricultural Research Service, Temple, Texas, USA.*
- 1028 Pettitt. (1979). A Non-parametric to the Approach Problem. *Applied Statistics*, 28(2), 126–135.  
 1029 <https://doi.org/doi: 10.2307/2346729>
- 1030 Rathjens, H., Bieger, K., Srinivasan, R., & Arnold, J. G. (2016). *CMhyd User Manual:*  
 1031 *Documentation for preparing simulated climate change data for hydrologic impact studies.*

- 1032 p.16p. [https://swat.tamu.edu/media/115265/bias\\_cor\\_man.pdf](https://swat.tamu.edu/media/115265/bias_cor_man.pdf)
- 1033 Sattari, M.-T., Joudi, A. R., & Kusiak, A. (2017). Assessment of different methods for estimation  
1034 of missing data in precipitation studies. *Hydrology Research*, 48(4), 1032–1044.  
1035 <https://doi.org/10.2166/nh.2016.364>
- 1036 Sen, P. K. (1968). Estimates of the Regression Coefficient Based on Kendall’s Tau. *Journal of*  
1037 *the American Statistical Association*, 63(324), 1379–1389.  
1038 <https://doi.org/10.1080/01621459.1968.104809>
- 1039 Serdeczny, O., Adams, S., Baarsch, F., Coumou, D., Robinson, A., Hare, W., Schaeffer, M.,  
1040 Perrette, M., & Reinhardt, J. (2017). Climate change impacts in Sub-Saharan Africa : from  
1041 physical changes to their social repercussions. *Regional Environmental Change*, 17, 1585–  
1042 1600. <https://doi.org/10.1007/s10113-015-0910-2>
- 1043 Shigute, M., Alamirew, T., Abebe, A., Ndehedehe, C. E., & Kassahun, H. T. (2022).  
1044 Understanding Hydrological Processes under Land Use Land Cover Change in the Upper  
1045 Genale River Basin , Ethiopia. *Water*, 14(23), 3881. <https://doi.org/10.3390/w14233881>
- 1046 Shigute, M., Alamirew, T., Abebe, A., Ndehedehe, C. E., & Kassahun, H. T. (2023). Analysis of  
1047 rainfall and temperature variability for agricultural water management in the upper Genale  
1048 river basin , Ethiopia. *Scientific African*, 20, e01635.  
1049 <https://doi.org/10.1016/j.sciaf.2023.e01635>
- 1050 Shrestha, M., Acharya, S. C., & Shrestha, P. K. (2017). Bias correction of climate models for  
1051 hydrological modelling – are simple methods still useful? *Meteorological Applications*,  
1052 24(3), 531–539. <https://doi.org/10.1002/met.1655>
- 1053 Shrestha, S. (2014). *Climate Change Impacts and Adaptation in Water Resources and Water Use*  
1054 *Sectors: Case Studies from Southeast Asia*. Springer International Publishing.  
1055 <https://doi.org/10.1007/978-3-319-09746-6>
- 1056 Shukla, S., & Gedam, S. (2018). Assessing the impacts of urbanization on hydrological  
1057 processes in a semi-arid river basin of Maharashtra , India. *Modeling Earth Systems and*  
1058 *Environment*, 4(2), 699–728. <https://doi.org/10.1007/s40808-018-0446-9>
- 1059 Syukuro, M. (2019). Role of greenhouse gas in climate change\*\*. *Tellus A: Dynamic*  
1060 *Meteorology and Oceanography*, 71(1), 1–13.  
1061 <https://doi.org/10.1080/16000870.2019.1620078>
- 1062 Takele, G. S., Gebre, G. S., Gebremariam, A. G., & Engida, A. N. (2022). Hydrological  
1063 modeling in the Upper Blue Nile basin using soil and water analysis tool (SWAT).  
1064 *Modeling Earth Systems and Environment*, 8(1), 277–292. <https://doi.org/10.1007/s40808-021-01085-9>
- 1066 Takele, G. S., Gebrie, G. S., Gebremariam, A. G., & Engida, A. N. (2022). Future climate  
1067 change and impacts on water resources in the Upper Blue Nile basin. *Journal of Water and*  
1068 *Climate Change*, 13(2), 908–925. <https://doi.org/10.2166/wcc.2021.235>
- 1069 Taylor, S. D., He, Y., & Hiscock, K. M. (2016). Modelling the impacts of agricultural  
1070 management practices on river water quality in Eastern England. *Journal of Environmental*  
1071 *Management*, 180, 147–168. <https://doi.org/10.1016/j.jenvman.2016.05.002>

- 1072 Teklay, A., Dile, Y. T., Asfaw, D. H., & Bayabil, H. K. (2020). Impacts of Climate and Land  
 1073 Use Change on Hydrological Response in Gumara watershed, Ethiopia. *Ecohydrology &*  
 1074 *Hydrobiology*, 21(2), 315–322. <https://doi.org/10.1016/j.ecohyd.2020.12.001>
- 1075 Tessema, N., Kebede, A., & Yadeta, D. (2021). Modelling the effects of climate change on  
 1076 streamflow using climate and hydrological models: the case of the Kesem sub-basin of the  
 1077 Awash River basin, Ethiopia. *International Journal of River Basin Management*, 19(4),  
 1078 469–480. <https://doi.org/10.1080/15715124.2020.1755301>
- 1079 Teutschbein, C., & Seibert, J. (2012). *Bias correction of regional climate model simulations for*  
 1080 *hydrological climate-change impact studies : Review and evaluation of different methods.*  
 1081 457, 12–29. <https://doi.org/10.1016/j.jhydrol.2012.05.052>
- 1082 Theil, H. (1950). *A rank-invariant method of linear and polynomial analysis, part 3.* Nederlandse  
 1083 Akademie van Wetenschappen. Proceedings 53, 1397–1412.
- 1084 van Buuren, S., & Groothuis-Oudshoorn, K. (2011). mice: Multivariate imputation by chained  
 1085 equations in R. *Journal of Statistical Software*, 45(3), 1–67.  
 1086 <https://doi.org/10.18637/jss.v045.i03>
- 1087 von Neumann, J. (1941). Distribution of the ratio of the mean square successive difference to the  
 1088 variance. *The Annals of Mathematical Statistics*, 12(4), 367–395.  
 1089 <https://doi.org/doi:10.1214/aoms/1177731677>
- 1090 Welborn, L. (2018). Africa and climate change Projecting vulnerability and adaptive capacity.  
 1091 *Institute for Security Studies, November*, 1–24.  
 1092 <https://issafrica.s3.amazonaws.com/site/uploads/ar14.pdf>
- 1093 Worku, G., Teferi, E., Bantider, A., & Dile, Y. T. (2020). Statistical bias correction of regional  
 1094 climate model simulations for climate change projection in the Jemma sub-basin, upper  
 1095 Blue Nile Basin of Ethiopia. *Theoretical and Applied Climatology*, 139(3), 1569–1588.  
 1096 <https://doi.org/10.1007/s00704-019-03053-x>
- 1097 Worku, G., Teferi, E., Bantider, A., & Dile, Y. T. (2021). Modelling hydrological processes  
 1098 under climate change scenarios in the Jemma Sub-basin of upper Blue Nile Basin , Ethiopia.  
 1099 *Climate Risk Management*, 31, 100272. <https://doi.org/10.1016/j.crm.2021.100272>
- 1100 Worqlul, A. W., Dile, Y. T., Ayana, E. K., & Jeong, J. (2018). Impact of Climate Change on  
 1101 Streamflow Hydrology in Headwater Catchments of the Upper Blue Nile. *Water*, 10, 120.  
 1102 <https://doi.org/10.3390/w10020120>
- 1103 Yeboah, K. A., Akpoti, K., Kabo-bah, A. T., Ofosu, E. A., Siabi, E. K., Mortey, E. M., &  
 1104 Okyereh, S. A. (2022). Assessing climate change projections in the Volta Basin using the  
 1105 CORDEX-Africa climate simulations and statistical bias-correction. *Environmental*  
 1106 *Challenges*, 6, 100439. <https://doi.org/10.1016/j.envc.2021.100439>
- 1107 Zhang, B., Shrestha, N. K., Daggupati, P., Rudra, R., & Shukla, R. (2018). Quantifying the  
 1108 Impacts of Climate Change on Streamflow Dynamics of Two Major Rivers of the Northern  
 1109 Lake Erie Basin in Canada. *Sustainability*, 10(8), 2897. <https://doi.org/10.3390/su10082897>
- 1110